

**A neural network-assisted 3D theoretical thermoelastic solution for laminated liquid crystal elastomer plate used in restoring cardiac mechanical function**

Wang, Jue ; Yuan, Weiyi; Li, Zichuan; Trofimov, Yuri; Lishik, Sergey; Fan, Jiajie

**DOI**

[10.1016/j.jmbbm.2022.105478](https://doi.org/10.1016/j.jmbbm.2022.105478)

**Publication date**

2022

**Document Version**

Final published version

**Published in**

Journal of the mechanical behavior of biomedical materials

**Citation (APA)**

Wang, J., Yuan, W., Li, Z., Trofimov, Y., Lishik, S., & Fan, J. (2022). A neural network-assisted 3D theoretical thermoelastic solution for laminated liquid crystal elastomer plate used in restoring cardiac mechanical function. *Journal of the mechanical behavior of biomedical materials*, 136, Article 105478. <https://doi.org/10.1016/j.jmbbm.2022.105478>

**Important note**

To cite this publication, please use the final published version (if applicable).  
Please check the document version above.

**Copyright**

Other than for strictly personal use, it is not permitted to download, forward or distribute the text or part of it, without the consent of the author(s) and/or copyright holder(s), unless the work is under an open content license such as Creative Commons.

**Takedown policy**

Please contact us and provide details if you believe this document breaches copyrights.  
We will remove access to the work immediately and investigate your claim.

***Green Open Access added to TU Delft Institutional Repository***

***'You share, we take care!' - Taverne project***

**<https://www.openaccess.nl/en/you-share-we-take-care>**

Otherwise as indicated in the copyright section: the publisher is the copyright holder of this work and the author uses the Dutch legislation to make this work public.



# A neural network-assisted 3D theoretical thermoelastic solution for laminated liquid crystal elastomer plate used in restoring cardiac mechanical function

Jue Wang<sup>a</sup>, Weiyi Yuan<sup>a</sup>, Zichuan Li<sup>d</sup>, Yuri Trofimov<sup>e</sup>, Sergey Lishik<sup>e</sup>, Jiajie Fan<sup>b,c,d,f,\*</sup>

<sup>a</sup> College of Mechanical & Electrical Engineering, Hohai University, Changzhou, 213022, China

<sup>b</sup> Institute of Future Lighting, Academy for Engineering & Technology, Fudan University, Shanghai, 200433, China

<sup>c</sup> State Key Laboratory of Applied Optics, Changchun Institute of Optics, Fine Mechanics and Physics, Chinese Academy of Sciences, Changchun, 130033, China

<sup>d</sup> Department of Microelectronics, Delft University of Technology, 2628 CD, Delft, the Netherlands

<sup>e</sup> Center of LED and Optoelectronic Technologies of NAS Belarus, Minsk, 220090, Belarus

<sup>f</sup> Fudan Zhangjiang Institute, Shanghai, 201203, China

## ARTICLE INFO

### Keywords:

Liquid crystal elastomer  
Laminated plate  
Thermoelastic theory  
Exact solution  
Neural network

## ABSTRACT

Some atrial contractile assist devices applied on the heart surface can be regarded as a laminated Liquid crystal elastomer (LCE) plate under steady temperature loads and a contact mechanical force. An exact solution for the deformation of the laminated LCE plate under combined thermal and mechanical loads is derived by solving the three-dimensional (3D) equilibrium equations including heat conduction and thermoelastic theory. The validity of mathematical formula and computer programming is proved by convergence and comparison examples with finite element method (FEM). In order to simplify the complex calculation of exact solution, a back propagation neural network (BPNN) is further trained with a database containing 9504 sets of thermo-mechanical load conditions and their corresponding deformation which is solved by the exact solutions. Then the deformations of LCE plate subject to combined thermo-mechanical load can be predicted by this BP neural network instead of complex numerical calculation. Moreover, it is also applied to inverse the contact mechanical force at the bottom surface of LCE plate with a given deformation and temperature conditions. The results show that: (1) The results from the exact theoretical solution are in consistence with that from FEM but have a higher computational efficiency and stability; (2) The deformation of the laminated plate is more sensitive to the layered thickness of LCE than the variation of the temperature; (3) 3-D elasticity solutions of a laminated LCE plate under the combined thermos-mechanical load can be effectively predicted by a trained BP neural network.

## 1. Introduction

Mechanical atrial contractile assist device is one of the most effective medical instruments to solve the physical health problems for weakening or losing of cardiac mechanical function. The idea of using biocompatible polymers as actuators to support or restore cardiac mechanical function has become a hot spot in the design and manufacture of contractile assist devices. Liquid crystal elastomer (LCE) is a smart biomedical material and has negative thermal expansion characteristics. It could produce contraction or relaxation movement like muscle tissue under the external stimulation, such as light and heat (Ahn et al., 2019). However, LCE is usually composited with some flexible substrates to satisfy some practical requirements (Lu et al., 2019; Liu et al., 2020). Cui

et al. presented a simple analytical thermo-mechanical model for LCE bilayer structures, which is one dimensional solution along the thickness direction (Yun et al., 2018). Therefore, it has scientific and engineering significance to obtain the 3-D elasticity solutions of laminated LCE plates under mechanical contact load and in a thermal load from the human body.

The mechanical atrial contractile assist devices can be regarded as a 3-D layered composite LCE plate under thermo-mechanical loads. Considerable efforts have been devoted to the analysis of mechanical models of plate based on various theories, which are represented by classical plate theory (CPT) (Wu, 2016; Jia et al., 2013), first-order shear deformation theory (FSDT) (Jonnalagadda et al., 1994; Nguyen et al., 2019) and higher-order shear deformation theory (HDST) (Kumar et al.,

\* Corresponding author. Institute of Future Lighting, Academy for Engineering & Technology, Fudan University.

E-mail address: [jiajie.fan@fudan.edu.cn](mailto:jiajie.fan@fudan.edu.cn) (J. Fan).

<https://doi.org/10.1016/j.jmbbm.2022.105478>

Received 7 July 2022; Received in revised form 16 September 2022; Accepted 18 September 2022

Available online 2 October 2022

1751-6161/© 2022 Elsevier Ltd. All rights reserved.

2011; Zhang and Selim, 2017). CPT refers to a theoretical model of plate performance based on Kirchhoff's hypothesis, which has certain advantages and can be applied to a reasonable range of applications. Koruche et al. (Koruche and Patil, 2015) applied CPT to establish a theoretical model to show the mechanical response of a laminated plate with different thermo-mechanical loading conditions. However, CPT ignores the effect of transverse shear deformation, so that it overestimates the stiffness of the plate (Sadrnejad, 2009). To this end, Mindlin (Mindlin, 1951; Shimpi et al., 2018) added a correction coefficient to the shear stress and proposed FSDT. FSDT considered the influence of shear deformation. It assumed that the longitudinal displacement was linear and the lateral displacement was constant. Bellifa (Bellifa Benrahou et al., 2016) and Zhang (Zhang et al., 2016) et al. used the concepts of FSDT to derive the equilibrium equations of functionally graded plates and laminated nanocomposite plates respectively. The shear correction coefficient in FSDT is a constant. However, the determination of this coefficient is not easy since it relies on the parameters of materials and loading conditions (Reddy et al., 2014). Therefore, HDST was proposed and applied to describe the transverse displacements with polynomial functions to skip the step of determining the shear correction factor (Ferreira et al., 2003). Abdelaziz (Abdelaziz et al., 2011) proposed a displacement-based high-order shear deformation theory to study the response of functionally graded laminated plates under a steady state. Furthermore, the Carrera's Unified Formulation (CUF) (Carrera et al., 2011) uses  $N$ -order polynomials to expand the displacement variables on the thickness coordinates and reduces a 3-D problem to a bidimensional one to realize the process of various plate and shell theories. Therefore, the influence of transverse normal strain can also be analyzed. Nali (Nali et al., 2011) and Ramos et al. (2016) used CUF to analyze multilayered and laminated composite plates under thermal load.

Different from the above CPT, FSDT, HDST and their extensions, there are no hypotheses in the governing equation of 3-D elastic theory. The exact mechanical solutions of the plates using the strict 3-D elastic theory can acquire higher accuracy (Eslami et al., 2013). Zenkour (2015) established an accurate 3-D solution model of temperatures, displacements and stresses of single-layer thermal shock plate based on thermoelastic theory. Xu et al. (2010) proposed an approximate analytical solution of a simply supported plate with inhomogeneous thickness under combined thermal and mechanical loads with the 3-D thermoelastic theory. Vel et al. (Vel and Batra, 2002) studied the 3-D deformation of a simply supported functionally graded plate through thermoelastic theory. The above studies have established the analytical model of single-layer plate by using the thermoelastic theory, which has laid a theoretical foundation for the establishment of the analytical model of laminated plate. Qian et al. (2014) applied the 3-D thermoelastic theory to obtain the elastic solution of a simply supported laminated plate under temperature load. Zhang et al. (2021) proposed the analytical solution of temperature, displacements and stresses of laminated rectangular plate with material temperature dependence.

It should be noted that the research achievements mentioned above provided different methods for obtaining the mechanical solutions of both single layer and laminated plates under different loads. However, the complex derivation and calculation process seriously limits its practicability. Therefore, it is very important to find a simple way to obtain the relative relationship between laminated plates' mechanical load and deformation in temperature field. As a result, engineers can predict the deformations conveniently and efficiently without the original cumbersome calculation, as well as inverse the mechanical loads applied on the laminated plate based on the measured deformation. Artificial neural network (ANN) imitates the self-learning of human brain which can independently detect and extract the correlation between data (Keles et al., 2016). It is composed of many integrated processing units called neurons that used for data classification, prediction and cluster (Esfe et al., 2015). Back propagation (BP) network is the most extensive model of ANN. It can output specific prediction results

based on the mapping relationship obtained through learning and training input parameters. Sung et al. (Choi et al., 2003) used an ANN model to predict the split growth of notched composite laminates. Reddy et al. (2013) predicted deformation and stress of laminated plate under uniformly distributed load through BP neural network by training of 322 sets of data. Ataya et al. (Ayata et al., 2006) calculated the temperature distribution on the surface of metal substrate composed of layered copper and aluminum by finite element method. Based on these data, the temperature distribution of metal substrate alloys with different thickness is predicted by ANN. Wang et al. (2022) used the exact 2-D thermoelastic model of laminated beam to establish a BP neural network database containing 561 sets of data for predicting the mechanical solutions of laminated beam. It would be of significance to apply the BP neural network to predict the mechanical properties of 3-D laminated plates under combined thermo-mechanical loads.

For the advantages of ANN in data analysis and prediction, a BP neural network is proposed to estimate the mechanical solution of a laminated plate under combined thermal and mechanical loads. The dataset required for training and testing for the BP neural network is obtained by developing exact solutions based on the 3-D heat conduction and thermoelastic theory. The convergence and comparison with FEM are studies to ensure the accuracy of original training data. Parametric investigations are carried out for the influence of temperature and layer thickness on the plate deformation. BP neural networks show the effectiveness of predicting the deformation of LCE plate according to the known load conditions, as well as inverting the mechanical loads according to the measured deformation. The verification of the prediction and inversion results is presented to shown the accuracy.

## 2. Theoretical model

### 2.1. Exact mechanical model for a laminated LCE plate

#### 2.1.1. Solution of the temperature field

A rectangular laminated LCE plate as shown in Fig. 1(a) with the size of  $a \times b \times H$  is modelled as a simply supported 3-D plate with  $p$  layers. The  $i$ -th layer plate is described in a local coordinate system  $x - y - \bar{z}$  as shown in Fig. 1(b)  $h^{(i)}$  is the thickness of each layer.  $h^{(i)}$  is the thickness of  $i$ -th layer. The laminated plate can be composed of different materials in each layer. The material properties in the  $i$ -th is described by elastic modulus  $E^{(i)}$ , Poisson ratio  $\mu^{(i)}$ , thermal expansion coefficients  $\alpha^{(i)}$ , and thermal conductivity  $k^{(i)}$ . Temperature loads  $T_t(x, y)$  and  $T_b(x, y)$  are applied on top and bottom surfaces of the LCE plate, respectively. In addition,  $q(x, y)$  is the mechanical load applied on the bottom surface of the plate. The laminated plate is simply-supported on four sides as shown in Fig. 1(c).

In the local coordinate system, the temperature field  $T^{(i)}(x, y, \bar{z})$  of the  $i$ -th layer is satisfied by a 3-D heat conduction equation:

$$\frac{\partial^2 T^{(i)}(x, y, \bar{z})}{\partial x^2} + \frac{\partial^2 T^{(i)}(x, y, \bar{z})}{\partial y^2} + \frac{\partial^2 T^{(i)}(x, y, \bar{z})}{\partial \bar{z}^2} = 0 \quad (1)$$

### 2.2. The thermal boundary conditions of the laminated plate are

$$T^{(i)}(0, y, \bar{z}) = T_i(a, y, \bar{z}) = 0 \quad (2a)$$

$$T^{(i)}(x, 0, \bar{z}) = T^{(i)}(x, b, \bar{z}) = 0 \quad (2b)$$

According to Eq. (2), the solution of Eq. (1) can be expanded in Fourier series:

$$T^{(i)}(x, y, \bar{z}) = \sum_{m=1}^{\infty} \sum_{n=1}^{\infty} t_{mn}^{(i)}(\bar{z}) \sin \frac{m\pi x}{a} \sin \frac{n\pi y}{b} \quad (3)$$

Substituting Eq. (3) is into Eq. (1), the expression of  $t_{mn}^{(i)}(\bar{z})$  can be solved as

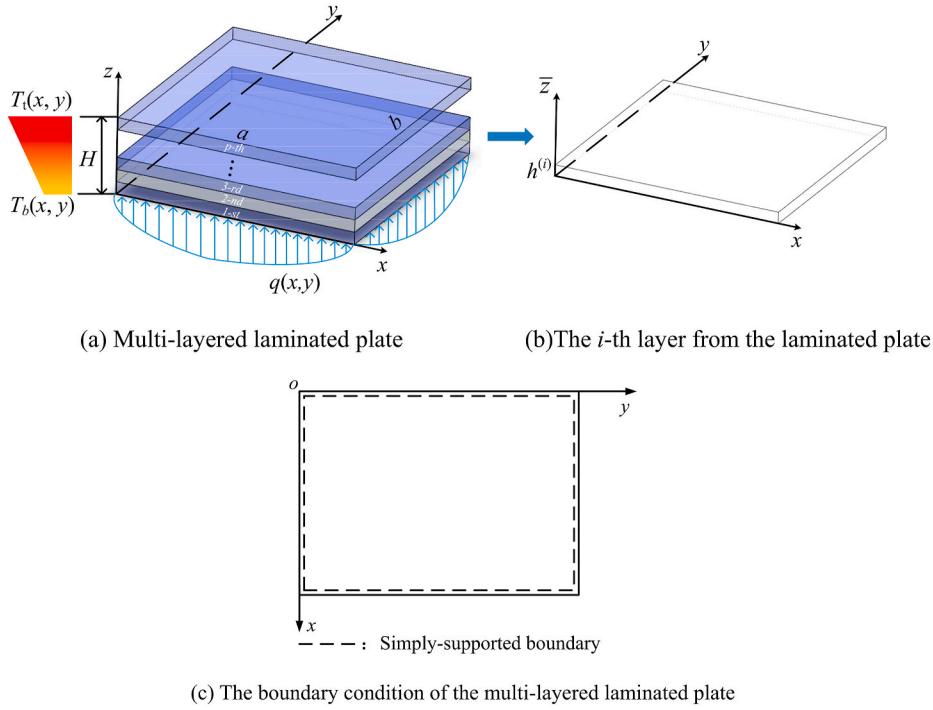


Fig. 1. Schematic diagram of 3-D laminated plate subjected to combined thermo-mechanical load.

$$T^{(i)}(x, y, \bar{z}) = \sum_{m=1}^{\infty} \sum_{n=1}^{\infty} \frac{n\pi}{b} \left[ e^{\beta_{mn}\bar{z}} \quad e^{-\beta_{mn}\bar{z}} \right] [XH_{mn}^{(i)}]_{2 \times 1} \sin \frac{m\pi x}{a} \sin \frac{n\pi y}{b} \quad (4)$$

where  $\beta_{mn} = \sqrt{\left(\frac{m\pi}{a}\right)^2 + \left(\frac{n\pi}{b}\right)^2}$ .  $XH_{mn}^{(i)} = [G_{mn}^{(i)} \quad H_{mn}^{(i)}]^T$  is a matrix with unknown coefficients. It depends on the boundary conditions of temperatures of the  $i$ -th layer. The two unknown coefficients will be subsequently obtained by the derivation and transfer matrix formula according to continuous conditions.

The temperature field and heat flux of each layer can be written as:

$$\begin{bmatrix} T^{(i)}(x, y, \bar{z}) \\ k^{(i)} \frac{\partial T^{(i)}(x, y, \bar{z})}{\partial \bar{z}} \end{bmatrix} = \sum_{m=1}^{\infty} \sum_{n=1}^{\infty} K_{mn}^{(i)}(\bar{z}) \sin \frac{m\pi x}{a} \sin \frac{n\pi y}{b} \quad (5)$$

Combining Eqs. (4) and (5), we can get:

$$K_{mn}^{(i)}(\bar{z}) = C_{mn}^{(i)}(\bar{z}) XH_{mn}^{(i)} \quad (6)$$

in which

$$C_{mn}^{(i)}(\bar{z}) = \begin{bmatrix} \frac{n\pi}{b} e^{\beta_{mn}\bar{z}} & \frac{n\pi}{b} e^{-\beta_{mn}\bar{z}} \\ k^{(i)} \frac{n\pi}{b} \beta_{mn} e^{\beta_{mn}\bar{z}} & -k^{(i)} \frac{n\pi}{b} \beta_{mn} e^{-\beta_{mn}\bar{z}} \end{bmatrix}.$$

Taking the values of  $\bar{z}$  in Eq. (6) as 0 and  $h^{(i)}$  respectively, we have  $K_{mn}^{(i)}(h^{(i)}) = [C_{mn}^{(i)}(h^{(i)}) C_{mn}^{(i)}(0)^{-1}] K_{mn}^{(i)}(0)$ . The relationship of temperature field between adjacent layers satisfied by  $K_{mn}^{(i)}(h^{(i)}) = K_{mn}^{(i+1)}(0)$ . Therefore, the relationship obtained from the above conditions through the transfer matrix method is:

$$K_{mn}^{(i)}(h^{(i)}) = \left[ \prod_{j=i}^1 C_{mn}^{(j)}(h^{(j)}) C_{mn}^{(j)}(0)^{-1} \right] K_{mn}^{(1)}(0) \quad (7)$$

The relationship of the unknown coefficients between the first layer and the  $i$ -th can be obtained by combining Eq. (6) and Eq. (7):

$$XH_{mn}^{(i)} = C_{mn}^{(i)}(h^{(i)})^{-1} \left\{ \prod_{j=i}^1 C_{mn}^{(j)}(h^{(j)}) C_{mn}^{(j)}(0)^{-1} \right\} C_{mn}^{(1)}(0) XH_{mn}^{(1)} \quad (8)$$

Combined with Eq. (4), the temperature boundary conditions of the laminated plate are:

$$\begin{cases} T^{(1)}(x, y, 0) = \sum_{m=1}^{\infty} \sum_{n=1}^{\infty} \frac{n\pi}{b} (G_{mn}^{(1)} + H_{mn}^{(1)}) \sin \frac{m\pi x}{a} \sin \frac{n\pi y}{b} = t_1(x, y) \\ T^{(p)}(x, y, h^{(p)}) = \sum_{m=1}^{\infty} \sum_{n=1}^{\infty} \frac{n\pi}{b} (e^{\beta_{mn}h^{(p)}} G_{mn}^{(p)} + e^{-\beta_{mn}h^{(p)}} H_{mn}^{(p)}) \sin \frac{m\pi x}{a} \sin \frac{n\pi y}{b} = t_2(x, y) \end{cases} \quad (9)$$

Eq. (9) can be written in Fourier series:

$$\begin{cases} \frac{n\pi}{b} (G_{mn}^{(1)} + H_{mn}^{(1)}) = \frac{4}{ab} \int_0^a \int_0^b t_1(x, y) \sin \frac{m\pi x}{a} \sin \frac{n\pi y}{b} dy dx \\ \frac{n\pi}{b} (e^{\beta_{mn}h^{(p)}} G_{mn}^{(p)} + e^{-\beta_{mn}h^{(p)}} H_{mn}^{(p)}) = \frac{4}{ab} \int_0^a \int_0^b t_2(x, y) \sin \frac{m\pi x}{a} \sin \frac{n\pi y}{b} dy dx \end{cases} \quad (10)$$

$XH_{mn}^{(1)}$  and  $XH_{mn}^{(p)}$  can be solved by Eq. (8) and Eq. (10) with  $i = p$ . Then the unknown coefficient matrix  $XH_{mn}^{(i)}$  of arbitrary  $i$ -th layer can be obtained by submitting  $XH_{mn}^{(1)}$  into Eq. (8). Finally, the temperature at any position inside the laminated plate can be obtained by substituting  $XH_{mn}^{(i)}$  into Eq. (4).

### 2.2.1. Solutions of the displacement and stress fields

In the local coordinate system  $x - y - \bar{z}$ , a set of 3-D thermoelastic constitutive equations of the  $i$ -th layer has

$$\begin{aligned}
\sigma_x^{(i)}(x, y, \bar{z}) &= (\lambda^{(i)} + 2G^{(i)}) \frac{\partial u^{(i)}(x, y, \bar{z})}{\partial x} + \lambda^{(i)} \frac{\partial v^{(i)}(x, y, \bar{z})}{\partial y} + \lambda^{(i)} \frac{\partial w^{(i)}(x, y, \bar{z})}{\partial \bar{z}} - (3\lambda^{(i)} + 2G^{(i)}) \alpha^{(i)} T^{(i)}(x, y, \bar{z}), \\
\sigma_y^{(i)}(x, y, \bar{z}) &= (\lambda^{(i)} + 2G^{(i)}) \frac{\partial v^{(i)}(x, y, \bar{z})}{\partial y} + \lambda^{(i)} \frac{\partial u^{(i)}(x, y, \bar{z})}{\partial x} + \lambda^{(i)} \frac{\partial w^{(i)}(x, y, \bar{z})}{\partial \bar{z}} - (3\lambda^{(i)} + 2G^{(i)}) \alpha^{(i)} T^{(i)}(x, y, \bar{z}), \\
\sigma_{\bar{z}}^{(i)}(x, y, \bar{z}) &= (\lambda^{(i)} + 2G^{(i)}) \frac{\partial w^{(i)}(x, y, \bar{z})}{\partial \bar{z}} + \lambda^{(i)} \frac{\partial u^{(i)}(x, y, \bar{z})}{\partial x} + \lambda^{(i)} \frac{\partial v^{(i)}(x, y, \bar{z})}{\partial y} - (3\lambda^{(i)} + 2G^{(i)}) \alpha^{(i)} T^{(i)}(x, y, \bar{z}), \\
\tau_{xy}^{(i)}(x, y, \bar{z}) &= G^{(i)} \left( \frac{\partial u^{(i)}(x, y, \bar{z})}{\partial y} + \frac{\partial v^{(i)}(x, y, \bar{z})}{\partial x} \right), \\
\tau_{y\bar{z}}^{(i)}(x, y, \bar{z}) &= G^{(i)} \left( \frac{\partial v^{(i)}(x, y, \bar{z})}{\partial \bar{z}} + \frac{\partial w^{(i)}(x, y, \bar{z})}{\partial y} \right), \\
\tau_{x\bar{z}}^{(i)}(x, y, \bar{z}) &= G^{(i)} \left( \frac{\partial u^{(i)}(x, y, \bar{z})}{\partial \bar{z}} + \frac{\partial w^{(i)}(x, y, \bar{z})}{\partial x} \right)
\end{aligned} \tag{11}$$

where  $\sigma_x^{(i)}$ ,  $\sigma_y^{(i)}$  and  $\sigma_{\bar{z}}^{(i)}$  represent the  $i$ -th layer's normal stresses.  $\tau_{xy}^{(i)}$ ,  $\tau_{y\bar{z}}^{(i)}$  and  $\tau_{x\bar{z}}^{(i)}$  represent the shear stresses.  $u^{(i)}$ ,  $v^{(i)}$  and  $w^{(i)}$  represent three displacement components.  $G^{(i)}$  is the shear modulus.  $\lambda^{(i)}$  is Lamé constant with  $\lambda^{(i)} = \frac{E^{(i)}\mu^{(i)}}{(\mu^{(i)}+1)(1-2\mu^{(i)})}$ .

By substituting Eq. (11) into the 3-D elastic theoretical equilibrium equation, we have:

$$\begin{aligned}
u^{(i)}(x, y, \bar{z}) &= \sum_{m=1}^{\infty} \sum_{n=1}^{\infty} U_{mn}^{(i)}(\bar{z}) \cos \frac{m\pi x}{a} \sin \frac{n\pi y}{b}, \\
v^{(i)}(x, y, \bar{z}) &= \sum_{m=1}^{\infty} \sum_{n=1}^{\infty} V_{mn}^{(i)}(\bar{z}) \sin \frac{m\pi x}{a} \cos \frac{n\pi y}{b}, \\
w^{(i)}(x, y, \bar{z}) &= \sum_{m=1}^{\infty} \sum_{n=1}^{\infty} W_{mn}^{(i)}(\bar{z}) \sin \frac{m\pi x}{a} \sin \frac{n\pi y}{b}
\end{aligned} \tag{14}$$

$$\begin{aligned}
&(\lambda^{(i)} + 2G^{(i)}) \frac{\partial^2 u^{(i)}(x, y, \bar{z})}{\partial x^2} + G^{(i)} \frac{\partial^2 u^{(i)}(x, y, \bar{z})}{\partial y^2} + G^{(i)} \frac{\partial^2 u^{(i)}(x, y, \bar{z})}{\partial \bar{z}^2} + (\lambda^{(i)} + G^{(i)}) \frac{\partial^2 v^{(i)}(x, y, \bar{z})}{\partial x \partial y} \\
&+ (\lambda^{(i)} + G^{(i)}) \frac{\partial^2 w^{(i)}(x, y, \bar{z})}{\partial x \partial \bar{z}} = (3\lambda^{(i)} + 2G^{(i)}) \alpha^{(i)} \frac{\partial T^{(i)}(x, y, \bar{z})}{\partial x}, \\
&(\lambda^{(i)} + 2G^{(i)}) \frac{\partial^2 v^{(i)}(x, y, \bar{z})}{\partial y^2} + G^{(i)} \frac{\partial^2 v^{(i)}(x, y, \bar{z})}{\partial x^2} + G^{(i)} \frac{\partial^2 v^{(i)}(x, y, \bar{z})}{\partial \bar{z}^2} + (\lambda^{(i)} + G^{(i)}) \frac{\partial^2 u^{(i)}(x, y, \bar{z})}{\partial x \partial y} \\
&+ (\lambda^{(i)} + G^{(i)}) \frac{\partial^2 w^{(i)}(x, y, \bar{z})}{\partial y \partial \bar{z}} = (3\lambda^{(i)} + 2G^{(i)}) \alpha^{(i)} \frac{\partial T^{(i)}(x, y, \bar{z})}{\partial y}, \\
&(\lambda^{(i)} + 2G^{(i)}) \frac{\partial^2 w^{(i)}(x, y, \bar{z})}{\partial \bar{z}^2} + G^{(i)} \frac{\partial^2 w^{(i)}(x, y, \bar{z})}{\partial x^2} + G^{(i)} \frac{\partial^2 w^{(i)}(x, y, \bar{z})}{\partial y^2} + (\lambda^{(i)} + G^{(i)}) \frac{\partial^2 u^{(i)}(x, y, \bar{z})}{\partial x \partial \bar{z}} \\
&+ (\lambda^{(i)} + G^{(i)}) \frac{\partial^2 v^{(i)}(x, y, \bar{z})}{\partial y \partial \bar{z}} = (3\lambda^{(i)} + 2G^{(i)}) \alpha^{(i)} \frac{\partial T^{(i)}(x, y, \bar{z})}{\partial \bar{z}}
\end{aligned} \tag{12}$$

The force and displacement boundary conditions are:

$$\begin{aligned}
\sigma_x^{(i)}(0, y, \bar{z}) &= \sigma_x^{(i)}(a, y, \bar{z}) = 0, \\
\sigma_y^{(i)}(0, y, \bar{z}) &= \sigma_y^{(i)}(a, y, \bar{z}) = 0, \\
v^{(i)}(0, y, \bar{z}) &= v^{(i)}(a, y, \bar{z}) = w^{(i)}(0, y, \bar{z}) = w^{(i)}(a, y, \bar{z}) = 0, \\
u^{(i)}(x, 0, \bar{z}) &= u^{(i)}(x, b, \bar{z}) = w^{(i)}(x, 0, \bar{z}) = w^{(i)}(x, b, \bar{z}) = 0
\end{aligned} \tag{13}$$

According to Eq. (13), the displacement solution of the  $i$ -th layer's can be expanded as

The expressions of  $U_{mn}^{(i)}(\bar{z})$ ,  $V_{mn}^{(i)}(\bar{z})$  and  $W_{mn}^{(i)}(\bar{z})$  can be obtained by substituting Eq. (4) together with Eq. (14) into Eq. (12). Then, the  $i$ -th layer's displacement field is expressed as following matrix form:

$$\begin{aligned}
\begin{bmatrix} u^{(i)}(x, y, \bar{z}) \\ v^{(i)}(x, y, \bar{z}) \\ w^{(i)}(x, y, \bar{z}) \end{bmatrix} &= \sum_{m=1}^{\infty} \sum_{n=1}^{\infty} \{ [DU_{mn}^{(i)}]_{3 \times 6} [XD_{mn}^{(i)}]_{6 \times 1} + [DH_{mn}^{(i)}]_{3 \times 2} [XH_{mn}^{(i)}]_{2 \times 1} \} \\
&\odot \begin{bmatrix} \cos \frac{m\pi x}{a} \sin \frac{n\pi y}{b} \\ \sin \frac{m\pi x}{a} \cos \frac{n\pi y}{b} \\ \sin \frac{m\pi x}{a} \sin \frac{n\pi y}{b} \end{bmatrix}
\end{aligned} \tag{15}$$

where  $\odot$  is Hadamard product.  $\mathbf{XD}_{mn}^{(i)} = [\mathbf{A}_{mn}^{(i)} \ \mathbf{B}_{mn}^{(i)} \ \mathbf{C}_{mn}^{(i)} \ \mathbf{D}_{mn}^{(i)} \ \mathbf{E}_{mn}^{(i)} \ \mathbf{F}_{mn}^{(i)}]^T$  is unknown coefficient matrix. The subsequent boundary conditions and the transfer matrix method according to continuous conditions of the adjacent layers can be used to obtain the unknown coefficient matrix.

Combined with Eq. (15) and Eq. (11), we have:

$$\mathbf{H}_{mn}^{(i)}(\bar{z}) = [\mathbf{U}_{mn}^{(i)}(\bar{z}) \ \mathbf{V}_{mn}^{(i)}(\bar{z}) \ \mathbf{W}_{mn}^{(i)}(\bar{z}) \ \mathbf{Z}_{mn}^{(i)}(\bar{z}) \ \mathbf{X}_{mn}^{(i)}(\bar{z}) \ \mathbf{Y}_{mn}^{(i)}(\bar{z})]^T = \mathbf{D}_{mn}^{(i)}(\bar{z}) \mathbf{XD}_{mn}^{(i)} + \mathbf{B}_{mn}^{(i)}(\bar{z}) \quad (18)$$

where the elements in the matrices  $\mathbf{D}_{mn}^{(i)}(\bar{z})$  and  $\mathbf{B}_{mn}^{(i)}(\bar{z})$  are consisted by some elements in  $\mathbf{DU}_{mn}^{(i)}$ ,  $\mathbf{DH}_{mn}^{(i)}$ ,  $\mathbf{SU}_{mn}^{(i)}$  and  $\mathbf{SH}_{mn}^{(i)}$  as follows:

$$\mathbf{D}_{mn}^{(i)}(\bar{z}) = \begin{bmatrix} \mathbf{DU}_{mn}^{(i)}(1,1) & \mathbf{DU}_{mn}^{(i)}(1,2) & \mathbf{DU}_{mn}^{(i)}(1,3) & \mathbf{DU}_{mn}^{(i)}(1,4) & \mathbf{DU}_{mn}^{(i)}(1,5) & \mathbf{DU}_{mn}^{(i)}(1,6) \\ \mathbf{DU}_{mn}^{(i)}(2,1) & \mathbf{DU}_{mn}^{(i)}(2,2) & \mathbf{DU}_{mn}^{(i)}(2,3) & \mathbf{DU}_{mn}^{(i)}(2,4) & \mathbf{DU}_{mn}^{(i)}(2,5) & \mathbf{DU}_{mn}^{(i)}(2,6) \\ \mathbf{DU}_{mn}^{(i)}(3,1) & \mathbf{DU}_{mn}^{(i)}(3,2) & \mathbf{DU}_{mn}^{(i)}(3,3) & \mathbf{DU}_{mn}^{(i)}(3,4) & \mathbf{DU}_{mn}^{(i)}(3,5) & \mathbf{DU}_{mn}^{(i)}(3,6) \\ \mathbf{SU}_{mn}^{(i)}(3,1) & \mathbf{SU}_{mn}^{(i)}(3,2) & \mathbf{SU}_{mn}^{(i)}(3,3) & \mathbf{SU}_{mn}^{(i)}(3,4) & \mathbf{SU}_{mn}^{(i)}(3,5) & \mathbf{SU}_{mn}^{(i)}(3,6) \\ \mathbf{SU}_{mn}^{(i)}(4,1) & \mathbf{SU}_{mn}^{(i)}(4,2) & \mathbf{SU}_{mn}^{(i)}(4,3) & \mathbf{SU}_{mn}^{(i)}(4,4) & \mathbf{SU}_{mn}^{(i)}(4,5) & \mathbf{SU}_{mn}^{(i)}(4,6) \\ \mathbf{SU}_{mn}^{(i)}(5,1) & \mathbf{SU}_{mn}^{(i)}(5,2) & \mathbf{SU}_{mn}^{(i)}(5,3) & \mathbf{SU}_{mn}^{(i)}(5,4) & \mathbf{SU}_{mn}^{(i)}(5,5) & \mathbf{SU}_{mn}^{(i)}(5,6) \end{bmatrix}, \mathbf{B}_{mn}^{(i)}(\bar{z}) = \begin{bmatrix} \mathbf{DH}_{mn}^{(i)}(1,1) & \mathbf{DH}_{mn}^{(i)}(1,2) \\ \mathbf{DH}_{mn}^{(i)}(2,1) & \mathbf{DH}_{mn}^{(i)}(2,2) \\ \mathbf{DH}_{mn}^{(i)}(3,1) & \mathbf{DH}_{mn}^{(i)}(3,2) \\ \mathbf{SH}_{mn}^{(i)}(3,1) & \mathbf{SH}_{mn}^{(i)}(3,2) \\ \mathbf{SH}_{mn}^{(i)}(4,1) & \mathbf{SH}_{mn}^{(i)}(4,2) \\ \mathbf{SH}_{mn}^{(i)}(5,1) & \mathbf{SH}_{mn}^{(i)}(5,2) \end{bmatrix} \mathbf{XH}_{mn}^{(i)}.$$

$$\begin{bmatrix} \sigma_x^{(i)}(x, y, \bar{z}) \\ \sigma_y^{(i)}(x, y, \bar{z}) \\ \sigma_z^{(i)}(x, y, \bar{z}) \\ \tau_{xz}^{(i)}(x, y, \bar{z}) \\ \tau_{yz}^{(i)}(x, y, \bar{z}) \\ \tau_{xy}^{(i)}(x, y, \bar{z}) \end{bmatrix} = \sum_{m=1}^{\infty} \sum_{n=1}^{\infty} \{ [\mathbf{SU}_{mn}^{(i)}]_{6 \times 6} [\mathbf{XD}_{mn}^{(i)}]_{6 \times 1} + [\mathbf{SH}_{mn}^{(i)}]_{6 \times 2} [\mathbf{XH}_{mn}^{(i)}]_{2 \times 1} \} \odot \begin{bmatrix} \sin \frac{m\pi x}{a} \sin \frac{n\pi y}{b} \\ \sin \frac{m\pi x}{a} \sin \frac{n\pi y}{b} \\ \sin \frac{m\pi x}{a} \sin \frac{n\pi y}{b} \\ \cos \frac{m\pi x}{a} \sin \frac{n\pi y}{b} \\ \sin \frac{m\pi x}{a} \cos \frac{n\pi y}{b} \\ \cos \frac{m\pi x}{a} \cos \frac{n\pi y}{b} \end{bmatrix} \quad (16)$$

The expressions of the elements in matrices  $\mathbf{DU}_{mn}^{(i)}$ ,  $\mathbf{DH}_{mn}^{(i)}$ ,  $\mathbf{SU}_{mn}^{(i)}$  and  $\mathbf{SH}_{mn}^{(i)}$  are shown in Appendix.

The matrix combining Eq. (15) and Eq. (16) has:

$$\begin{bmatrix} u^{(i)}(x, y, \bar{z}) \\ v^{(i)}(x, y, \bar{z}) \\ w^{(i)}(x, y, \bar{z}) \\ \sigma_z^{(i)}(x, y, \bar{z}) \\ \tau_{xz}^{(i)}(x, y, \bar{z}) \\ \tau_{yz}^{(i)}(x, y, \bar{z}) \end{bmatrix} = \sum_{m=1}^{\infty} \sum_{n=1}^{\infty} \mathbf{H}_{mn}^{(i)}(\bar{z}) \odot \begin{bmatrix} \cos \frac{m\pi x}{a} \sin \frac{n\pi y}{b} \\ \sin \frac{m\pi x}{a} \cos \frac{n\pi y}{b} \\ \sin \frac{m\pi x}{a} \sin \frac{n\pi y}{b} \\ \sin \frac{m\pi x}{a} \sin \frac{n\pi y}{b} \\ \cos \frac{m\pi x}{a} \sin \frac{n\pi y}{b} \\ \sin \frac{m\pi x}{a} \cos \frac{n\pi y}{b} \end{bmatrix} \quad (17)$$

where

According to Eq. (18), we have  $\mathbf{H}_{mn}^{(i)}(h^{(i)}) = \mathbf{D}_{mn}^{(i)}(h^{(i)}) \{ \mathbf{D}_{mn}^{(i)}(0)^{-1} [\mathbf{H}_{mn}^{(i)}(0) - \mathbf{B}_{mn}^{(i)}(0)] \} + \mathbf{B}_{mn}^{(i)}(h^{(i)})$ . According to the continuity condition between adjacent layers  $\mathbf{H}_{mn}^{(i)}(h^{(i)}) = \mathbf{H}_{mn}^{(i+1)}(0)$ , the relationships obtained from the above conditions through the matrix transfer method is:

$$\mathbf{H}_{mn}^{(i)}(h^{(i)}) = \begin{bmatrix} U1_{mn} & U2_{mn} \\ U3_{mn} & U4_{mn} \end{bmatrix} \mathbf{H}_{mn}^{(1)}(0) + [\mathbf{S}_{mn}]_{6 \times 1} \quad (19)$$

where  $\begin{bmatrix} U1_{mn} & U2_{mn} \\ U3_{mn} & U4_{mn} \end{bmatrix} = \prod_{i=p}^1 \mathbf{D}_{mn}^{(i)}(h^{(i)}) \mathbf{D}_{mn}^{(i)}(0)^{-1}$ ,  $\mathbf{S}_{mn} = -$

$$\sum_{j=1}^p \left\{ \prod_{i=p}^j [\mathbf{D}_{mn}^{(i)}(h^{(i)}) \mathbf{D}_{mn}^{(i)}(0)^{-1}] \right\} \mathbf{B}_{mn}^{(j)}(0) + \sum_{j=2}^p \left\{ \prod_{i=p}^j [\mathbf{D}_{mn}^{(i)}(h^{(i)}) \mathbf{D}_{mn}^{(i)}(0)^{-1}] \right\} \mathbf{B}_{mn}^{(j-1)}(h^{(j-1)}) + \mathbf{B}_{mn}^{(p)}(h^{(p)}).$$

### 2.3. The stress boundary conditions of the laminate plate are

$$\begin{aligned} \sigma_z^{(1)}(x, y, 0) &= q(x, y), \tau_{xz}^{(1)}(x, y, 0) = 0, \tau_{yz}^{(1)}(x, y, 0) = 0, \\ \sigma_z^{(p)}(x, y, h_p) &= 0, \tau_{xz}^{(p)}(x, y, h_p) = 0, \tau_{yz}^{(p)}(x, y, h_p) = 0 \end{aligned} \quad (20)$$

The mechanical load  $q(x, y)$  forced at the bottom surface of the laminated plate could be expressed by Fourier series as follows:

$$q(x, y) = \sum_{m=1}^{\infty} \sum_{n=1}^{\infty} q_{mn} \sin \frac{m\pi x}{a} \sin \frac{n\pi y}{b} \quad (21)$$

with

$$q_{mn} = \frac{4}{ab} \int_0^b \int_0^a q(x, y) \sin \frac{m\pi x}{a} \sin \frac{n\pi y}{b} dx dy \quad (22)$$

Substituting Eq. (20) and Eq. (17) into Eq. (19), we have



$$\begin{bmatrix} U_{mn}^{(p)}(h^{(p)}) \\ V_{mn}^{(p)}(h^{(p)}) \\ W_{mn}^{(p)}(h^{(p)}) \\ 0 \\ 0 \\ 0 \end{bmatrix} = \begin{bmatrix} U1_{mn} & U2_{mn} \\ U3_{mn} & U4_{mn} \end{bmatrix} \begin{bmatrix} U_{mn}^{(1)}(0) \\ V_{mn}^{(1)}(0) \\ W_{mn}^{(1)}(0) \\ \frac{4}{ab} \int_0^b \int_0^a q(x,y) \sin \frac{m\pi x}{a} \sin \frac{n\pi y}{b} dx dy \\ 0 \\ 0 \end{bmatrix} + S_{mn} \quad (23)$$

Then, Eq. (23) is decomposed into two third-order matrix equations as follows:

$$\begin{bmatrix} U_{mn}^{(p)}(h^{(p)}) \\ V_{mn}^{(p)}(h^{(p)}) \\ W_{mn}^{(p)}(h^{(p)}) \end{bmatrix} = U1_{mn} \begin{bmatrix} U_{mn}^{(1)}(0) \\ V_{mn}^{(1)}(0) \\ W_{mn}^{(1)}(0) \end{bmatrix} + U2_{mn} \begin{bmatrix} \frac{4}{ab} \int_0^b \int_0^a q(x,y) \sin \frac{m\pi x}{a} \sin \frac{n\pi y}{b} dx dy \\ 0 \\ 0 \end{bmatrix} + \begin{bmatrix} S_{mn}(1,1) \\ S_{mn}(2,1) \\ S_{mn}(3,1) \end{bmatrix} \quad (24)$$

$$\begin{bmatrix} 0 \\ 0 \\ 0 \end{bmatrix} = U3_{mn} \begin{bmatrix} U_{mn}^{(1)}(0) \\ V_{mn}^{(1)}(0) \\ W_{mn}^{(1)}(0) \end{bmatrix} + U4_{mn} \begin{bmatrix} \frac{4}{ab} \int_0^b \int_0^a q(x,y) \sin \frac{m\pi x}{a} \sin \frac{n\pi y}{b} dx dy \\ 0 \\ 0 \end{bmatrix} + \begin{bmatrix} S_{mn}(4,1) \\ S_{mn}(5,1) \\ S_{mn}(6,1) \end{bmatrix} \quad (25)$$

$U_{mn}^{(1)}(0)$ ,  $V_{mn}^{(1)}(0)$  and  $W_{mn}^{(1)}(0)$  can be obtained by solving Eq. (25). Then, the displacements and stresses  $H_{mn}^{(i)}(h^{(i)})$  can be solved by substituting  $U_{mn}^{(1)}(0)$ ,  $V_{mn}^{(1)}(0)$  and  $W_{mn}^{(1)}(0)$  into Eq. (19). The following formula is obtained by combining Eq. (18) and Eq. (19):

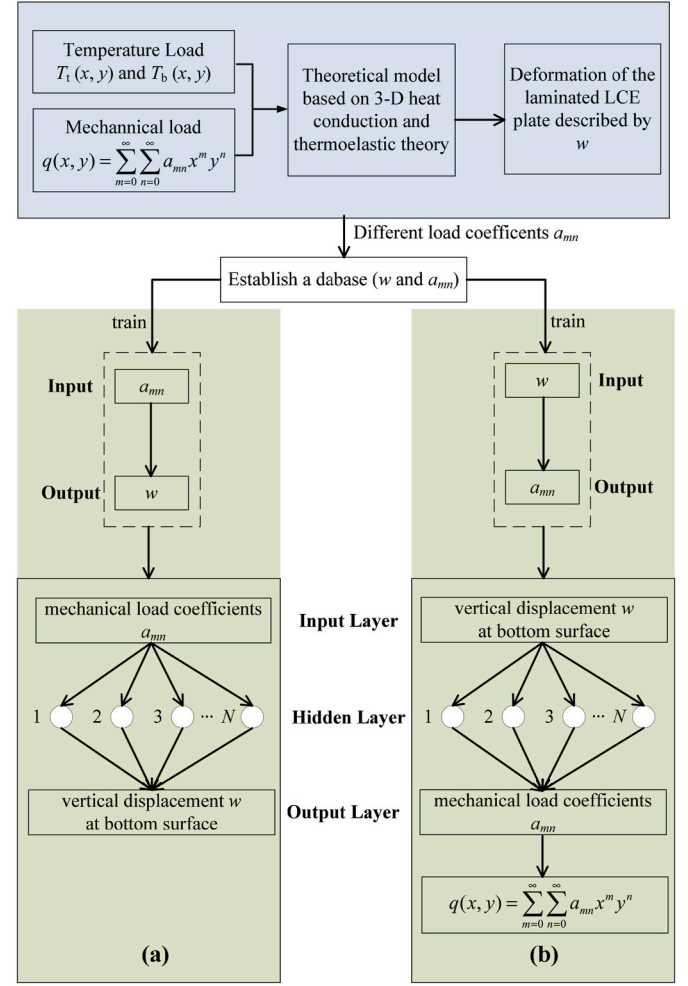


**Fig. 2.** The architecture of the BP prediction: (a) prediction of the deformation induced by the mechanical load; (b) inversion of the mechanical load according to the deformation.

$$XD_{mn}^{(i)} = D_{mn}^{(i)}(h^{(i)})^{-1} \left\{ \begin{bmatrix} U1_{mn} & U2_{mn} \\ U3_{mn} & U4_{mn} \end{bmatrix} \begin{bmatrix} U_{mn}^{(1)}(0) \\ V_{mn}^{(1)}(0) \\ W_{mn}^{(1)}(0) \\ \frac{4}{ab} \int_0^b \int_0^a q(x,y) \sin \frac{m\pi x}{a} \sin \frac{n\pi y}{b} dx dy \\ 0 \\ 0 \end{bmatrix} + S_{mn} - B_{mn}^{(i)}(h^{(i)}) \right\} \quad (26)$$

Through the matrix operation of Eq. (26), the matrix of undetermined coefficients  $XD_{mn}^{(i)}$  in each laminated layer can be obtained. Finally, the displacements and stresses at any position in the laminated plate subjected to thermo-mechanical load can be obtained by substituting these coefficients  $XD_{mn}^{(i)}$  into Eq. (17).

#### 2.4. Architecture of a BP neural network

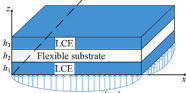
As an atrial contractile assist device, the surface mechanical load of the LCE plate in a temperature field and its corresponding deformation are important parameters to evaluate its mechanical properties. The exact solution based on the above theoretical model can effectively calculate the deformation of a laminated LCE plate under the combined thermo-mechanical loads through the complex algebra and integral



**Table 1**  
Material parameters of laminated LCE plate in numerical examples.

Materials	Young's modulus (MPa)	Poisson's ratio	Coefficient of thermal expansion ( $^{\circ}\text{C}^{-1}$ )	Thermal conductivity ( $\text{W}/(\text{m}\cdot^{\circ}\text{C})$ )
LCE	6	0.499	$-1.5 \times 10^{-4}$	0.22
Flexible substrate	$4 \times 10^3$	0.34	$2.5 \times 10^{-5}$	0.12

**Table 2**  
Convergence of displacements under different mechanical loads in a temperature field.

Laminated LCE model	$q(x, y)$ (Pa)	Position	Dis.	Expansion order $m$ and $n$ of Fourier series in Eq. (15)				
				5	15	25	35	45
	10	$x = 1.5 \text{ m}$ ,	$u \text{ (mm)}$	−0.0629	−0.0503	−0.0502	−0.0504	−0.0504
		$y = 0.5 \text{ m}$ ,	$v \text{ (mm)}$	−0.500	−0.510	−0.510	−0.510	−0.510
		$z = 0.1 \text{ m}$ ,	$w \text{ (}\mu\text{m)}$	−55.1	−57.0	−58.1	−58.2	−58.2
		$x = 3.0 \text{ m}$ ,	$u \text{ (mm)}$	0.154	0.179	0.179	0.179	0.179
		$y = 1.2 \text{ m}$ ,	$v \text{ (mm)}$	0.179	0.172	0.172	0.172	0.172
		$z = 0.2 \text{ m}$ ,	$w \text{ (}\mu\text{m)}$	64.1	62.8	64.0	64.1	64.1
	$x + y + 1$	$x = 1.5 \text{ m}$ ,	$u \text{ (mm)}$	−0.0629	−0.0503	−0.0502	−0.0504	−0.0504
		$y = 0.5 \text{ m}$ ,	$v \text{ (mm)}$	−0.500	−0.510	−0.510	−0.510	−0.510
		$z = 0.1 \text{ m}$ ,	$w \text{ (}\mu\text{m)}$	−56.8	−58.8	−59.8	−59.9	−59.9
		$x = 3.0 \text{ m}$ ,	$u \text{ (mm)}$	0.153	0.179	0.179	0.179	0.179
		$y = 1.2 \text{ m}$ ,	$v \text{ (mm)}$	0.179	0.172	0.172	0.172	0.172
		$z = 0.2 \text{ m}$ ,	$w \text{ (}\mu\text{m)}$	62.5	61.2	62.4	62.5	62.5
	$x^2 + y^2 + xy + x + y + 1$	$x = 1.5 \text{ m}$ ,	$u \text{ (mm)}$	−0.0628	−0.0502	−0.0502	−0.0503	−0.0503
		$y = 0.5 \text{ m}$ ,	$v \text{ (mm)}$	−0.500	−0.505	−0.510	−0.510	−0.510
		$z = 0.1 \text{ m}$ ,	$w \text{ (}\mu\text{m)}$	−55.1	−57.0	−58.1	−58.2	−58.2
		$x = 3.0 \text{ m}$ ,	$u \text{ (mm)}$	0.153	0.179	0.179	0.179	0.179
		$y = 1.2 \text{ m}$ ,	$v \text{ (mm)}$	0.179	0.172	0.172	0.172	0.172
		$z = 0.2 \text{ m}$ ,	$w \text{ (}\mu\text{m)}$	65.7	64.4	65.6	65.7	65.7

**Table 3**  
Comparison of the present displacements with FEM results at bottom surface under different mechanical loads in a temperature field.

$q(x, y)$ (Pa)	Dis	Method	$y = 0.6 \text{ m}, z = 0.2$					
			$x = 0 \text{ m}$	$x = 0.4 \text{ m}$	$x = 0.8 \text{ m}$	$x = 1.2 \text{ m}$	$x = 1.6 \text{ m}$	$x = 2 \text{ m}$
10	$u$ (mm)	Present	−0.66573	−0.40989	−0.21447	−0.10721	−0.044615	0
		FE	−0.66563	−0.41000	−0.21433	−0.10734	−0.044550	0
		Error	<b>0.015%</b>	<b>0.027%</b>	<b>0.065%</b>	<b>0.121%</b>	<b>0.150%</b>	<b>0%</b>
	$v$ (mm)	Present	0	−0.1848	−0.30926	−0.37822	−0.41146	−0.42127
		FE	0	−0.18482	−0.30929	−0.37824	−0.41148	−0.42128
		Error	<b>0%</b>	<b>0.011%</b>	<b>0.010%</b>	<b>0.005%</b>	<b>0.005%</b>	<b>0.002%</b>
	$z$ (μm)	Present	0	61.849	63.159	63.853	64.308	64.261
		FE	0	61.602	63.230	63.878	64.236	64.351
		Error	<b>0%</b>	<b>0.401%</b>	<b>0.112%</b>	<b>0.039%</b>	<b>0.112%</b>	<b>0.140%</b>
$x + y + 1$	$u$ (mm)	Present	−0.66593	−0.40969	−0.21421	−0.10735	−0.044595	0
		FE	−0.66552	−0.40991	−0.21427	−0.10730	−0.044540	0
		Error	<b>0.062%</b>	<b>0.054%</b>	<b>0.028%</b>	<b>0.047%</b>	<b>0.123%</b>	<b>0%</b>
	$v$ (mm)	Present	0	−0.18476	−0.30919	−0.37813	−0.41136	−0.42116
		FE	0	−0.18477	−0.30912	−0.37814	−0.41137	−0.42117
		Error	<b>0%</b>	<b>0.005%</b>	<b>0.023%</b>	<b>0.003%</b>	<b>0.002%</b>	<b>0.002%</b>
	$z$ (μm)	Present	0	60.777	61.866	62.110	62.234	62.316
		FE	0	60.776	61.786	62.060	62.253	62.368
		Error	<b>0%</b>	<b>0.002%</b>	<b>0.129%</b>	<b>0.081%</b>	<b>0.031%</b>	<b>0.083%</b>
$x^2 + y^2 + xy + x + y + 1$	$u$ (mm)	Present	−0.666	−0.40976	−0.21428	−0.10741	−0.044653	0
		FE	−0.66559	−0.40998	−0.21434	−0.10737	−0.044598	0
		Error	<b>0.061%</b>	<b>0.054%</b>	<b>0.028%</b>	<b>0.037%</b>	<b>0.123%</b>	<b>0%</b>
	$v$ (mm)	Present	0	−0.18479	−0.30926	−0.37822	−0.41148	−0.42131
		FE	0	−0.18480	−0.30927	−0.37823	−0.41149	−0.42132
		Error	<b>0%</b>	<b>0.005%</b>	<b>0.003%</b>	<b>0.003%</b>	<b>0.002%</b>	<b>0.002%</b>
	$z$ (μm)	Present	0	61.321	62.944	63.709	64.325	64.824
		FE	0	61.319	62.864	63.660	64.343	64.876
		Error	<b>0%</b>	<b>0.003%</b>	<b>0.127%</b>	<b>0.077%</b>	<b>0.028%</b>	<b>0.080%</b>

operations. However, the above exact solution cannot invert the surface mechanical load of the laminated LCE plate by a specific deformation. ANN is an information processing system composed of many connected neurons that can get the expected results in line with some rules on the basis of obtaining the mapping relationship between two multivariate information spaces (Baliyan et al., 2015). The common application of ANN is to train and learn the input database for predicting certain outputs. BP neural network has the highest efficiency in training. In this study, BP neural network is selected to predict the deformation or

mechanical load of a laminated LCE plate.

BP neural network is a static multi-layer forward ANN adopted the supervised learning method based on error back propagation algorithm and gradient descent method to minimize the mean square error. It usually includes three processes: (1) The input signal propagates forward, and the error with the sample value is calculated after the calculation and processing of the nodes of input layer and hidden layer; (2) The error signal is back propagated, and the weight as well as threshold are adjusted based on the learning rate in order to reduce the

error in gradient direction; (3) The input signal is continuously trained and learned until the error is reduced to the minimum mean square error or the training times reaches the maximum number of iterations. The required weight and threshold are obtained through finite iterative adjustment. Then the results of the given parameters are predicted. The training and prediction of BP neural network involved in this study are programmed and run by MATLAB software. In the training process, the training samples are firstly normalized by mapping them from original range to the range  $[-1, 1]$ . A newff function in Neural Network Toolbox of MATLAB is applied to construct the BP neural network model. The network parameters configured for training are  $\text{net.trainParam.epochs} = 1000$ ,  $\text{net.trainParam.lr} = 0.01$ ,  $\text{net.trainParam.goal} = 0.000001$ . In the prediction process, the test samples are normalized and then the  $\text{sim}$  function is used to simulate the trained BP neural network model. Finally, the simulation results are reversely normalized to obtain the prediction results.

The mechanical load is described by a two-dimensional Taylor polynomial function in Eq. (27). According to Taylor formula, with the different values and combinations of  $m$  and  $n$ ,  $q(x, y)$  can fit any mechanical load function with different continuous distribution.

$$q(x, y) = \sum_{m=0}^{\infty} \sum_{n=0}^{\infty} a_{mn} x^m y^n \quad (27)$$

where  $a_{mn}$  are the expansion coefficient of  $q(x, y)$ . BP neural network can be trained by a database composed of different mechanical load with expansion order  $m$ ,  $n$  and coefficients  $a_{mn}$ . The corresponding deformations of the laminated plates can be obtained by the exact solutions presented in section 2.1 under the conditions of given temperature and mechanical loads.

Fig. 2 shows the architecture of prediction of mechanical solutions.

Input layer, hidden layer and output layer constitute the basic structure of BP neural network. The node number of input and output layer depends on the composition of the input and output data, respectively. The training database is obtained from analytical solutions based on the presented 3-D thermoelastic mechanical model. Fig. 2(a) shows the BP neural network prediction of the deformation of the LCE plate under the action of mechanical load. The mechanical load coefficients  $a_{mn}$  are the input parameters while the deformation are the output parameters. Similarly, Fig. 2(b) shows the inversion of the mechanical load forced on LCE plate through the given elastic deformation. The displacements are the input parameters while mechanical load coefficients  $a_{mn}$  are the output parameters. The selecting node number  $M$  in the hidden layer can be determined based on an empirical formula as follows:

$$M = \sqrt{E + V} + Q \quad (28)$$

where  $M$ ,  $V$  and  $E$  are the node number in hidden layer, output layer and input layer, respectively.  $Q$  is the adjustment constant of the node number in hidden layer, with a value range of 1–10.

### 3. Results and discussion

#### 3.1. Convergence and comparison examples

The convergence the number of Fourier series and comparison with FEM are studies to confirm the correctness of exact mechanical solutions. A triple-layered laminated LCE plate is considered in this example. The triple-layered laminated LCE plate is a structure with the flexible substrate layer sandwiched between the two LCE layers on both sides. The geometrical size of the plate is  $4 \text{ m} \times 2 \text{ m} \times 0.3 \text{ m}$ . The layered thickness is  $h^{(1)} = h^{(2)} = h^{(3)} = 0.1 \text{ m}$ . Other parameters of materials

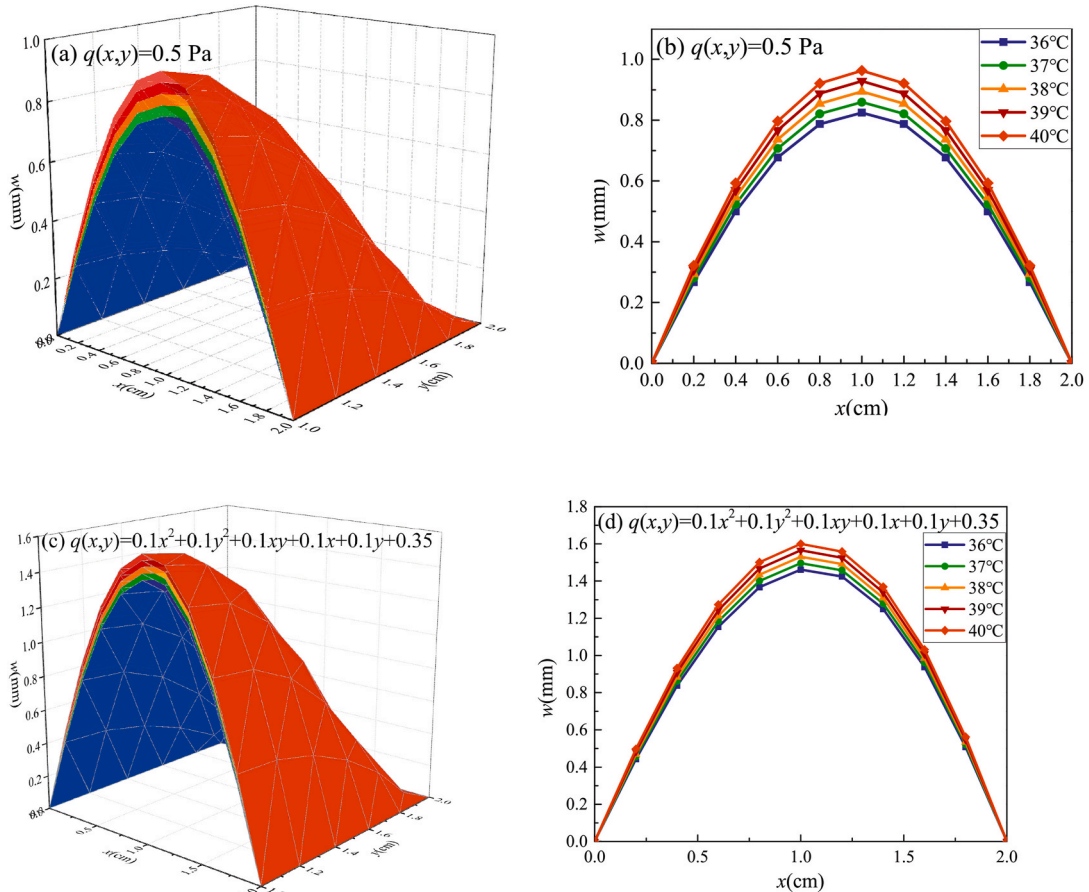


Fig. 3. The influence of temperature on the vertical displacement of laminated LCE plate.

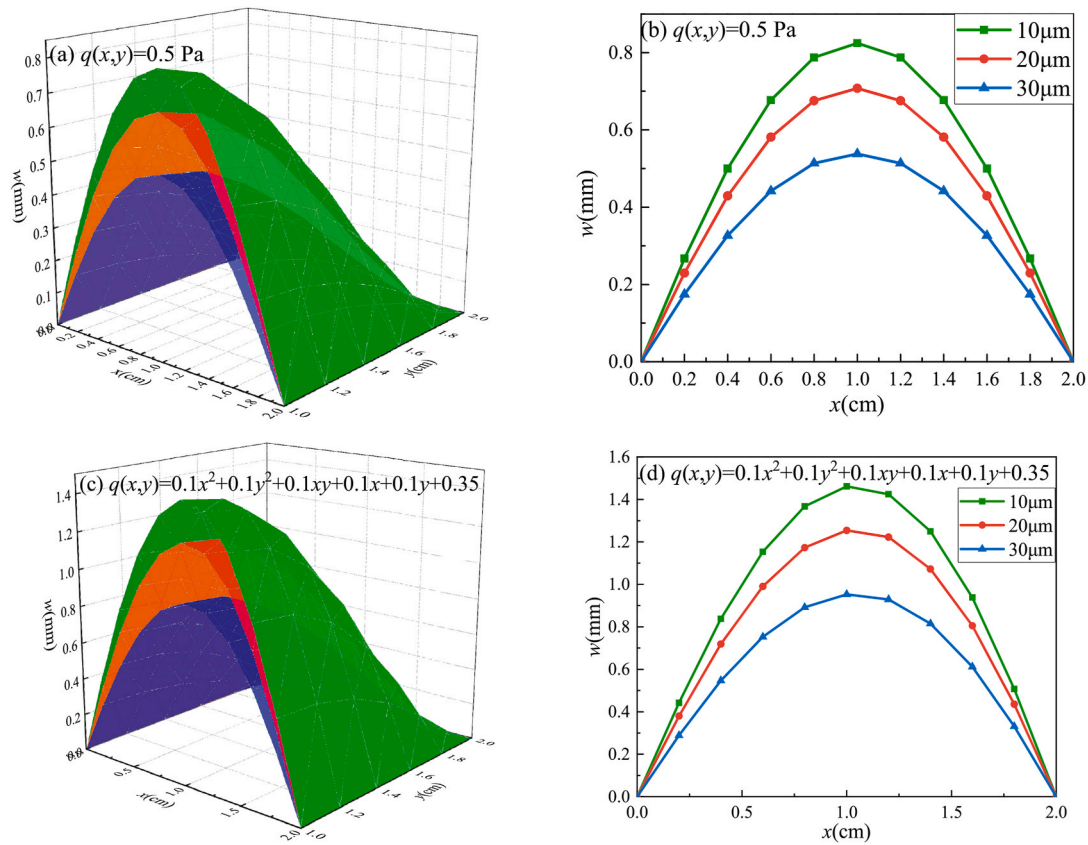


Fig. 4. The influence of LCE thickness on the vertical displacement of laminated LCE plate.

required in these studies are listed in Table 1. Constant temperature loads ( $T_b(x, y) = 36^\circ\text{C}$ ,  $T_t(x, y) = 36^\circ\text{C}$ ) are forced on the LCE plate.

Different  $m$  and  $n$  are selected in Table 2 to calculate the vertical displacement of some points in the LCE laminated plate and complete the convergence study of the analytical model. It can be seen from Table 2 that the results tend to be stable with the increase of  $m$  and  $n$ . It means that the vertical displacement is convergent. The expansion orders of Fourier series of  $m$  and  $n$  are both fixed at 35 in the subsequent numerical examples.

A finite element method (FEM) simulated by ANSYS software has been carried out to verify the effectiveness of formula derivation from Eq. (1) to Eq. (26) and its program coding. Table 3 shows the comparison between the present analytical results from 3-D thermoelastic theory and the numerical results from FEM in the cases for three different mechanical loads. The present exact theoretical solution is obtained from Eq. (17) incorporating with Eq. (26) and calculated by MATLAB

programming. The FEM model is simulated in ANSYS software by element SOLID5 which has eight nodes with up to six degrees of freedom at each node. SOLID5 has capacity for simulation of 3-D magnetic, thermal, electric, piezoelectric, and structural problem. Six different points in the laminated plate are selected for comparison. The  $y$ -axis and  $z$ -axis coordinates of these points are fixed at  $y = 0.6\text{ m}$  and  $z = 0.2\text{ m}$  respectively. The  $x$ -axis coordinates are fixed at  $0\text{ m}$ ,  $0.4\text{ m}$ ,  $0.8\text{ m}$ ,  $1.2\text{ m}$ ,  $1.6\text{ m}$  and  $2\text{ m}$ , respectively. The error between the vertical displacement results of present exact solution theory and FEM at each position in Table 3 is calculated by Eq. (29), in which the maximum relative error is less than 0.45%.

$$\text{error} = \left| \frac{J - I}{J} \right| \times 100\% \quad (29)$$

where  $J$  and  $I$  represent the results from FEM and the present theoretical model respectively.

Table 4

Calculation parameters used for establishing the database of the laminated LCE plate in a temperature field ( $T_b(x) = 36^\circ\text{C}$ ,  $T_t(x) = 37^\circ\text{C}$ ).

Point coordinates of the bottom surface ( $z = 0$ )	coefficient	Scale of coefficients
$x = 0.25\text{--}1.75\text{ cm}$ with a gradient of $0.25\text{ cm}$ ;	$a_{20}$	From 0 to 1 with a gradient of 0.1
$y = 0.25\text{--}1.75\text{ cm}$ with a gradient of $0.25\text{ cm}$ ;	$a_{02}$	From 0 to 0.7 with a gradient of 0.1
Vertical displacements of 49 points in total	$a_{11}$	From 0 to 0.01 with a gradient of 0.005
	$a_{10}$	From 0 to 0.1 with a gradient of 0.05
	$a_{01}$	From 0 to 0.1 with a gradient of 0.05
	$a_{00}$	From 0 to 1.5 with a gradient of 0.5

Table 5

Five groups of test sets for the verification of the prediction accuracy of BP neural network.

No.	Coefficients of mechanical load						Point coordinates of the bottom surface ( $z = 0$ )
	$a_{20}$	$a_{02}$	$a_{11}$	$a_{10}$	$a_{01}$	$a_{00}$	
#1	0	0	0	0	0	0.75	$x = 0.25\text{--}1.75\text{ cm}$ with a gradient of $0.25\text{ cm}$ ;
#2	0	0	0.01	0.5	0.2	0.5	$y = 0.25\text{--}1.75\text{ cm}$ with a gradient of $0.25\text{ cm}$ ;
#3	0.8	0.4	0.01	0.1	0	0.25	Vertical displacements of 49 points in total
#4	1.2	0.8	0.005	0.02	0.05	0.63	
#5	0.9	1	0	0	0	2	

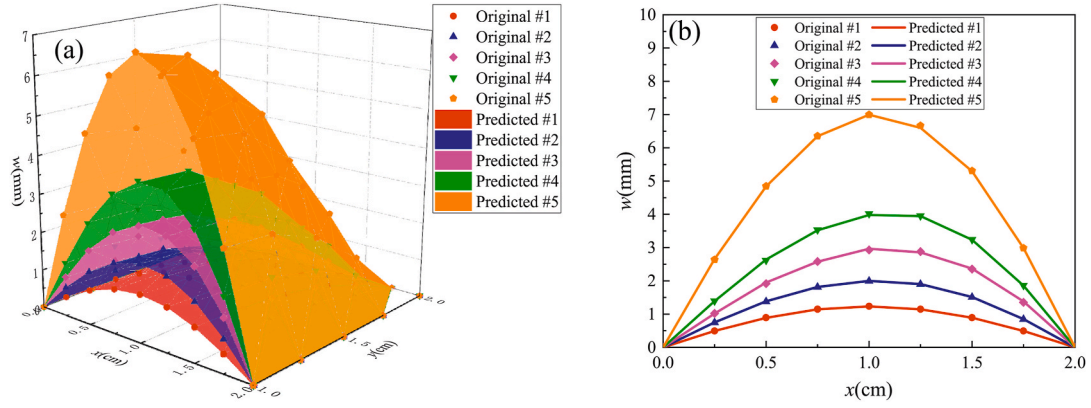


Fig. 5. Comparison of the vertical displacements between the results of the analytical solution and the prediction of the BP model.

### 3.2. Parametric studies

The influences of layer thickness and temperature on the displacement of laminated LCE plate are evaluated by following two examples. The material compositions of the plate are the same as that in section 3.1. The material parameters considered in the following examples are shown in Table 1. It is noticed that the coefficient of thermal expansion of LCE in Table 1 should have been varied with the temperature. However, since a small and low temperature range from 36 °C–40 °C is considered in the numerical example, the thermal expansion coefficient of LCE is assumed as a constant value for the simplification of the 3-D thermoelastic model. The length of the laminated LCE plate is a square with geometrical size 2.0 cm.

Fig. 3 demonstrates the effect of temperature on the deformation of a triple-layered laminated LCE plate. The thickness of each thin layer is 10  $\mu\text{m}$ . Body temperature is variable. Therefore, for simulation of the real situation in the human environment, the bottom surface temperature of the laminated LCE plate is kept at the normal human temperature (36 °C), and the top surface is under the temperature load from the normal human temperature to the fever temperature (36 °C–40 °C with a gradient of 1 °C). Fig. 3 shows that within the range of human body temperature, the displacement of laminated LCE plate increases with the increasing temperature. The calculated value of the exact solution indicates that the increase of the displacement at the centre part of laminated LCE plate is less than 4.2% with the increase of temperature of 1 °C. The results show that the change of human body temperature has minimal influence on the deformation of laminated LCE plate.

Fig. 4 demonstrates the effect of layered thickness of LCE on the

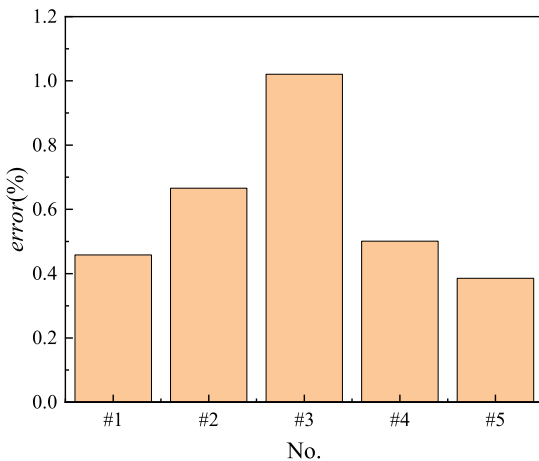


Fig. 6. The relative error of displacement between the BP model and the theoretical model.

deformation of the triple-layered laminated LCE plate. A temperature load of 36 °C is applied on the surfaces of the laminated LCE plate. The intermediate flexible substrate layer thickness is maintained at 10  $\mu\text{m}$ . LCE layer thickness is 10  $\mu\text{m}$ , 20  $\mu\text{m}$ , and 30  $\mu\text{m}$  respectively. As shown in Fig. 4, the effect of each LCE layer thickness is significant. When each layer thickness is 20  $\mu\text{m}$ , the displacement of the middle part of the structure decreases by more than 14.2% compared with that of each layer thickness is 10  $\mu\text{m}$ . When each layer thickness is 30  $\mu\text{m}$ , the displacement of the middle part of structure decreases by more than 24.0% compared with that of each layer thickness is 10  $\mu\text{m}$ . It indicates that the deformation of the laminate is more sensitive to the layer thickness of LCE than the temperature change. This is because that the elastic deformation of LCE layer is determined by its Young's modulus and Poisson's ratio and the thermal deformation of LCE layer is determined by its thermal conductivity and expansion. So due to the material properties, it seems that the elastic deformation of LCE laminated plate with its thickness between 10  $\mu\text{m}$  and 30  $\mu\text{m}$  is more significant than the thermal deformation caused by the temperature range of human body between 36 °C to 40 °C. Therefore, reducing the LCE layer thickness can significantly increase the deformation of laminated LCE plate.

### 3.3. Application of BP neural network prediction

In this study, the prediction of BP neural network includes the prediction of deformation and the inversion of mechanical load of laminated LCE plate with temperature load. The database for training BP neural network is made up of the surface mechanical load coefficients and corresponding displacements of laminated LCE plate. The temperature load is considered as  $T_b(x) = 36$  °C and  $T_t(x) = 37$  °C. In this study, a polynomial mechanical load function with six coefficients shown in Eq. (30) is selected.

$$q(x, y) = a_{00} + a_{10}x + a_{01}y + a_{11}xy + a_{20}x^2 + a_{02}y^2 \quad (30)$$

The selection of coefficients of mechanical load and the location of displacement investigation points are shown in Table 4 which is called training set with a total of 9504 groups of data. In addition, 5 groups of test set that are not part of the training data are listed in Table 5. It can test the feasibility and correctness of predicting mechanical solutions of laminated LCE plate based on the BP neural network.

The relative error between prediction results and exact results from theoretical model is expressed as follows for evaluation of the precision of prediction results:

$$\text{error} = \left| \frac{I - O}{I} \right| \times 100\% \quad (31)$$

where  $O$  and  $I$  represent the predicted result and the exact result, respectively.



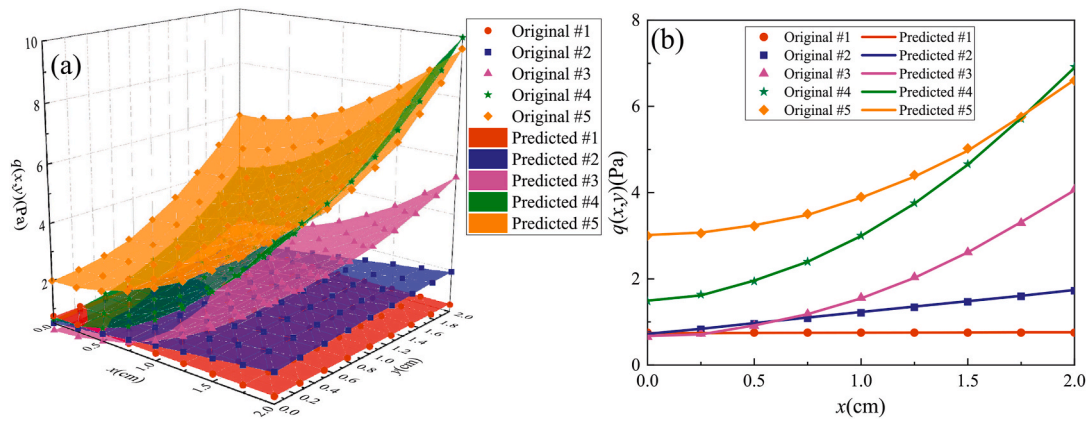


Fig. 7. Comparison between the inversed and actual mechanical loads.

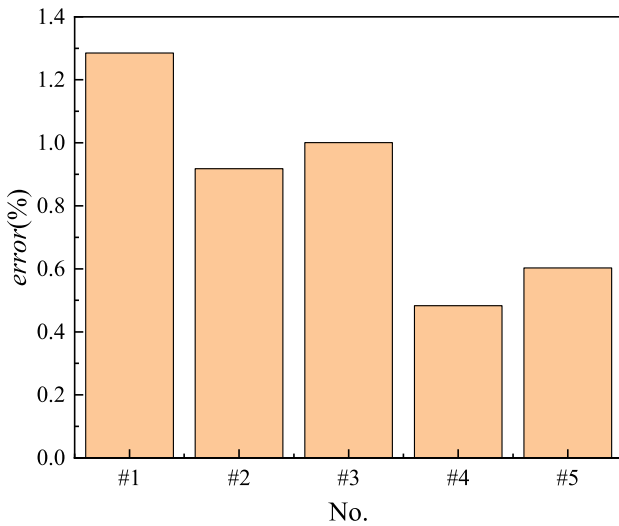


Fig. 8. The relative error between the inversed and actual mechanical loads.

### 3.3.1. Prediction of the deformation induced by thermos-mechanical load

The coefficients of the mechanical load  $a_{20}$ ,  $a_{02}$ ,  $a_{11}$ ,  $a_{10}$ ,  $a_{01}$ ,  $a_{00}$  in Eq. (30) are the input parameters. The vertical displacement  $w$  ( $w_1$ ,  $w_2$ , ...,  $w_{49}$ ) of 49 points as the output parameters. Therefore,  $E$  in Eq. (28) is 6 and  $V$  is 49. The adjustment constant is set as 3. Therefore, according to Eq. (28),  $M$  is 10.

In order to characterize the accuracy of displacement prediction, the coefficients of mechanical load of test sets in Table 5 are taken as the input data for prediction and accuracy analysis. Fig. 5 is used to intuitively show the fitting degree of the displacements between the exact theoretical results and the prediction results from BP model. Fig. 5(a) is a 3-D displacement distribution diagram for the symmetrical half of the laminated LCE plate. Fig. 5(b) shows the displacements distribution at  $y = 1$  cm. Fig. 5 shows that the predicted displacements and calculated displacements of the five sets of test data have highly consistence. Fig. 6 shows the error analysis of BP neural network in predicting vertical displacement. BP neural network can effectively predict the displacement of laminated LCE plate under mechanical loads in the temperature field with an average error of less than 1.1%.

### 3.3.2. Inversion of mechanical load according to the deformation

The vertical displacements  $w$  ( $w_1$ ,  $w_2$ , ...,  $w_{49}$ ) of 49 points are the input parameters. The coefficients  $a_{20}$ ,  $a_{02}$ ,  $a_{11}$ ,  $a_{10}$ ,  $a_{01}$ ,  $a_{00}$  in Eq. (30) are the output parameters. Therefore,  $E$  in Eq. (28) is 6 and  $V$  is 49. The adjustment constant is set as 5. Therefore,  $M$  is equal to 12 according to Eq. (28).

The displacements of test sets in Table 5 are taken as the input data for inversion of coefficients in Eq. (30) and accuracy analysis. Fig. 7 is used to intuitively show the comparison between the predicted mechanical loads and the actual mechanical loads. The comparison results show that the predicted mechanical loads are all consistent with the given ones. The prediction error shown in Fig. 8 indicated that the average error of predicting mechanical load is less than 1.3%. It also shows that BP neural network can effectively invert the mechanical load of a laminated LCE plate with specific displacements at the bottom surface.

## 4. Concluding remarks

A simple and effective approach is proposed for predicting mechanical solutions of laminated LCE plate under thermo-mechanical loads combining the theoretical model with BP neural network. The dataset required for training and testing the BP neural network is obtained by developing an exact theoretical model based on the 3-D heat conduction and thermoelastic theory. The convergence and comparison with FEM are studied to confirm the accuracy of original training data. The sensitivity of layer thickness and the temperature load to the deformation of LCE plate is assessed by parametric studies. The accuracy of the BP neural network is verified by comparing the prediction results with exact results. The following conclusions can be summarized as.

- (1) The error between the deformation results of the exact theoretical solution and the FEM is less than 0.45%, but the theoretical model has a higher computational efficiency and stability than FEM.
- (2) The LCE layer thickness play a more important role than the temperature variation does in terms of influence factor for the deformation of laminated LCE plate. LCE layer thickness can be reduced to improve the deformation performance of LCE laminated plate effectively.
- (3) The error of prediction and inversion of mechanical solution (deformation and surface mechanical load) of laminated LCE plate is less than 1.3%. It proves that BP neural network can effectively predict the mechanical solutions of laminated LCE plate under combined thermal and mechanical loads.

## Ethical statement

None.

## CRediT authorship contribution statement

Jue Wang: Writing – review & editing, Supervision, Resources,

Methodology, Funding acquisition, Formal analysis. **Weiye Yuan:** Writing – original draft, Visualization, Validation, Investigation, Formal analysis, Data curation. **Zichuan Li:** Writing – review & editing, Methodology. **Yuri Trofimov:** Writing – review & editing, Supervision. **Sergey Lishik:** Writing – review & editing, Supervision. **Jiajie Fan:** Supervision, Project administration, Funding acquisition, Conceptualization.

#### Declaration of competing interest

The authors declare that they have no known competing financial interests or personal relationships that could have appeared to influence the work reported in this paper.

#### Appendix

The expressions of the elements in matrix  $DU_{mn}^{(i)}$  are listed as:

$$DU_{mn}^{(i)}(1, 1) = 0$$

$$DU_{mn}^{(i)}(1, 2) = 0$$

$$DU_{mn}^{(i)}(1, 3) = \frac{mn\pi^2 \bar{z}}{ab\beta_{mn}} e^{\beta_{mn}\bar{z}}$$

$$DU_{mn}^{(i)}(1, 4) = -\frac{mn\pi^2 \bar{z}}{ab\beta_{mn}} e^{-\beta_{mn}\bar{z}}$$

$$DU_{mn}^{(i)}(1, 5) = \frac{\pi n}{b} e^{\beta_{mn}\bar{z}}$$

$$DU_{mn}^{(i)}(1, 6) = \frac{\pi n}{b} e^{-\beta_{mn}\bar{z}}$$

$$DU_{mn}^{(i)}(2, 1) = \beta_{mn} e^{\beta_{mn}\bar{z}}$$

$$DU_{mn}^{(i)}(2, 2) = -\beta_{mn} e^{-\beta_{mn}\bar{z}}$$

$$DU_{mn}^{(i)}(2, 3) = \left( \frac{\lambda^{(i)} + 3G^{(i)}}{\lambda^{(i)} + G^{(i)}} + \frac{n^2 \pi^2 \bar{z}}{b^2 \beta_{mn}} \right) e^{\beta_{mn}\bar{z}}$$

$$DU_{mn}^{(i)}(2, 4) = \left( \frac{\lambda^{(i)} + 3G^{(i)}}{\lambda^{(i)} + G^{(i)}} - \frac{n^2 \pi^2 \bar{z}}{b^2 \beta_{mn}} \right) e^{-\beta_{mn}\bar{z}}$$

$$DU_{mn}^{(i)}(2, 5) = -\frac{m\pi}{a} e^{\beta_{mn}\bar{z}}$$

$$DU_{mn}^{(i)}(2, 6) = -\frac{m\pi}{a} e^{-\beta_{mn}\bar{z}}$$

$$DU_{mn}^{(i)}(3, 1) = \frac{\pi n}{b} e^{\beta_{mn}\bar{z}}$$

$$DU_{mn}^{(i)}(3, 2) = \frac{\pi n}{b} e^{-\beta_{mn}\bar{z}}$$

$$DU_{mn}^{(i)}(3, 3) = \frac{\pi n}{b} z^{(i)} e^{\beta_{mn}\bar{z}}$$

$$DU_{mn}^{(i)}(3, 4) = \frac{\pi n}{b} z^{(i)} e^{-\beta_{mn}\bar{z}}$$

$$DU_{mn}^{(i)}(3, 5) = 0$$

$$DU_{mn}^{(i)}(3, 6) = 0$$

The expressions of the elements in matrix  $DH_{mn}^{(i)}$  are listed as:

$$DH_{mn}^{(i)}(1, 1) = -\frac{mn\pi^2}{ab\beta_{mn}^2} \frac{(3\lambda^{(i)} + 2G^{(i)})\alpha^{(i)}}{\lambda^{(i)} + G^{(i)}} e^{\beta_{mn}\bar{z}}$$

#### Data availability

The authors do not have permission to share data.

#### Acknowledgements

The financial supports from the National Natural Science Foundation of China (51805147, 52178474), Fundamental Research Funds for the Cornell University (B210202127), State Key Laboratory of Applied Optics (SKLAO2022001A01), Shanghai Science and Technology Development Foundation (21DZ2205200), Shanghai Pujiang Program (2021PJD002) and Natural Science Foundation of Jiangsu Province (BK20221233) are greatly acknowledged.

$$DH_{mn}^{(i)}(1, 2) = -\frac{mn\pi^2}{ab\beta_{mn}^2} \frac{(3\lambda^{(i)} + 2G^{(i)})\alpha^{(i)}}{\lambda^{(i)} + G^{(i)}} e^{-\beta_{mn}\bar{z}}$$

$$DH_{mn}^{(i)}(2, 1) = -\frac{n^2\pi^2}{b^2\beta_{mn}^2} \frac{(3\lambda^{(i)} + 2G^{(i)})\alpha^{(i)}}{\lambda^{(i)} + G^{(i)}} e^{\beta_{mn}\bar{z}}$$

$$DH_{mn}^{(i)}(2, 2) = -\frac{n^2\pi^2}{b^2\beta_{mn}^2} \frac{(3\lambda^{(i)} + 2G^{(i)})\alpha_i}{\lambda^{(i)} + G^{(i)}} e^{-\beta_{mn}\bar{z}}$$

$$DH_{mn}^{(i)}(3, 1) = 0$$

$$DH_{mn}^{(i)}(3, 2) = 0$$

The expressions of the elements in matrix  $SU_{mn}^{(i)}$  are listed as:

$$SU_{mn}^{(i)}(1, 1) = 0$$

$$SU_{mn}^{(i)}(1, 2) = 0$$

$$SU_{mn}^{(i)}(1, 3) = -\frac{2\pi n G^{(i)} e^{\beta_{mn}\bar{z}}}{b} \left( \frac{\lambda^{(i)}}{\lambda^{(i)} + G^{(i)}} + \frac{m^2\pi^2\bar{z}}{a^2\beta_{mn}} \right)$$

$$SU_{mn}^{(i)}(1, 4) = -\frac{2\pi n G^{(i)} e^{-\beta_{mn}\bar{z}}}{b} \left( \frac{\lambda^{(i)}}{\lambda^{(i)} + G^{(i)}} - \frac{m^2\pi^2\bar{z}}{a^2\beta_{mn}} \right)$$

$$SU_{mn}^{(i)}(1, 5) = -\frac{2mn\pi^2 G^{(i)}}{ab} e^{\beta_{mn}\bar{z}}$$

$$SU_{mn}^{(i)}(1, 6) = -\frac{2mn\pi^2 G^{(i)}}{ab} e^{-\beta_{mn}\bar{z}}$$

$$SU_{mn}^{(i)}(2, 1) = -\frac{2\pi n G^{(i)} \beta_{mn}}{b} e^{\beta_{mn}\bar{z}}$$

$$SU_{mn}^{(i)}(2, 2) = \frac{2\pi n G^{(i)} \beta_{mn}}{b} e^{-\beta_{mn}\bar{z}}$$

$$SU_{mn}^{(i)}(2, 3) = -\frac{2\pi n G^{(i)} e^{\beta_{mn}\bar{z}}}{b} \left( \frac{2\lambda^{(i)} + 3G^{(i)}}{\lambda^{(i)} + G^{(i)}} + \frac{n^2\pi^2\bar{z}}{b^2\beta_{mn}} \right)$$

$$SU_{mn}^{(i)}(2, 4) = -\frac{2\pi n G^{(i)} e^{-\beta_{mn}\bar{z}}}{b} \left( \frac{2\lambda^{(i)} + 3G^{(i)}}{\lambda^{(i)} + G^{(i)}} - \frac{n^2\pi^2\bar{z}}{b^2\beta_{mn}} \right)$$

$$SU_{mn}^{(i)}(2, 5) = -\frac{2mn\pi^2 G^{(i)}}{ab} e^{\beta_{mn}\bar{z}}$$

$$SU_{mn}^{(i)}(2, 6) = -\frac{2mn\pi^2 G^{(i)}}{ab} e^{-\beta_{mn}\bar{z}}$$

$$SU_{mn}^{(i)}(3, 1) = \frac{2\pi n G^{(i)} \beta_{mn}}{b} e^{\beta_{mn}\bar{z}}$$

$$SU_{mn}^{(i)}(3, 2) = -\frac{2\pi n G^{(i)} \beta_{mn}}{b} e^{-\beta_{mn}\bar{z}}$$

$$SU_{mn}^{(i)}(3, 3) = \frac{2\pi n G^{(i)} e^{\beta_{mn}\bar{z}}}{b} \left( \frac{G^{(i)}}{\lambda^{(i)} + G^{(i)}} + \beta_{mn}\bar{z} \right)$$

$$SU_{mn}^{(i)}(3, 4) = \frac{2\pi n G^{(i)} e^{-\beta_{mn}\bar{z}}}{b} \left( \frac{G^{(i)}}{\lambda^{(i)} + G^{(i)}} - \beta_{mn}\bar{z} \right)$$

$$SU_{mn}^{(i)}(3, 5) = 0$$

$$SU_{mn}^{(i)}(3, 6) = 0$$

$$SU_{mn}^{(i)}(4, 1) = \frac{mn\pi^2 G^{(i)}}{ab} e^{\beta_{mn}\bar{z}}$$



$$SU_{mn}^{(i)}(4, 2) = \frac{mn\pi^2 G^{(i)}}{ab} e^{-\beta_{mn}\bar{z}}$$

$$SU_{mn}^{(i)}(4, 3) = \frac{mn\pi^2 G^{(i)} e^{\beta_{mn}\bar{z}}}{ab} \left( \frac{1}{\beta_{mn}} + 2\bar{z} \right)$$

$$SU_{mn}^{(i)}(4, 4) = -\frac{mn\pi^2 G^{(i)} e^{-\beta_{mn}\bar{z}}}{ab} \left( \frac{1}{\beta_{mn}} - 2\bar{z} \right)$$

$$SU_{mn}^{(i)}(4, 5) = \frac{\pi n G^{(i)} \beta_{mn}}{b} e^{\beta_{mn}\bar{z}}$$

$$SU_{mn}^{(i)}(4, 6) = -\frac{\pi n G^{(i)} \beta_{mn}}{b} e^{-\beta_{mn}\bar{z}}$$

$$SU_{mn}^{(i)}(5, 1) = \left( \frac{n^2 \pi^2}{b^2} + \beta_{mn}^2 \right) G^{(i)} e^{\beta_{mn}\bar{z}}$$

$$SU_{mn}^{(i)}(5, 2) = \left( \frac{n^2 \pi^2}{b^2} + \beta_{mn}^2 \right) G^{(i)} e^{-\beta_{mn}\bar{z}}$$

$$SU_{mn}^{(i)}(5, 3) = \left( \frac{\lambda^{(i)} + 3G^{(i)}}{\lambda^{(i)} + G^{(i)}} \beta_{mn} + \frac{n^2 \pi^2}{b^2 \beta_{mn}} + \frac{2n^2 \pi^2 \bar{z}}{b^2} \right) G^{(i)} e^{\beta_{mn}\bar{z}}$$

$$SU_{mn}^{(i)}(5, 4) = -\left( \frac{\lambda^{(i)} + 3G^{(i)}}{\lambda^{(i)} + G^{(i)}} \beta_{mn} + \frac{n^2 \pi^2}{b^2 \beta_{mn}} - \frac{2n^2 \pi^2 \bar{z}}{b^2} \right) G^{(i)} e^{-\beta_{mn}\bar{z}}$$

$$SU_{mn}^{(i)}(5, 5) = -\frac{\pi m G^{(i)} \beta_{mn}}{a} e^{\beta_{mn}\bar{z}}$$

$$SU_{mn}^{(i)}(5, 6) = \frac{\pi m G^{(i)} \beta_{mn}}{a} e^{-\beta_{mn}\bar{z}}$$

$$SU_{mn}^{(i)}(6, 1) = \frac{m\pi G^{(i)}}{a} \beta_{mn} e^{\beta_{mn}\bar{z}}$$

$$SU_{mn}^{(i)}(6, 2) = -\frac{m\pi G^{(i)}}{a} \beta_{mn} e^{-\beta_{mn}\bar{z}}$$

$$SU_{mn}^{(i)}(6, 3) = \left( \frac{\lambda^{(i)} + 3G^{(i)}}{\lambda^{(i)} + G^{(i)}} \frac{m\pi}{a} + \frac{2mn^2 \pi^3 \bar{z}}{ab^2 \beta_{mn}} \right) G^{(i)} e^{\beta_{mn}\bar{z}}$$

$$SU_{mn}^{(i)}(6, 4) = \left( \frac{\lambda^{(i)} + 3G^{(i)}}{\lambda^{(i)} + G^{(i)}} \frac{m\pi}{a} - \frac{2mn^2 \pi^3 \bar{z}}{ab^2 \beta_{mn}} \right) G^{(i)} e^{-\beta_{mn}\bar{z}}$$

$$SU_{mn}^{(i)}(6, 5) = \left( \frac{n^2 \pi^2}{b^2} - \frac{m^2 \pi^2}{a^2} \right) G^{(i)} e^{\beta_{mn}\bar{z}}$$

$$SU_{mn}^{(i)}(6, 6) = \left( \frac{n^2 \pi^2}{b^2} - \frac{m^2 \pi^2}{a^2} \right) G^{(i)} e^{-\beta_{mn}\bar{z}}$$

The expressions of the elements in matrix  $\mathbf{SH}_{mn}^{(i)}$  are listed as:

$$SH_{mn}^{(i)}(1, 1) = -\frac{2\pi n G^{(i)} e^{\beta_{mn}\bar{z}}}{b} \frac{(3\lambda^{(i)} + 2G^{(i)})\alpha^{(i)}}{2\lambda^{(i)} + 2G^{(i)}} \frac{\left( \frac{n^2 \pi^2}{b^2} - \frac{m^2 \pi^2}{a^2} \right)}{\beta_{mn}^2}$$

$$SH_{mn}^{(i)}(1, 2) = -\frac{2\pi n G^{(i)} e^{-\beta_{mn}\bar{z}}}{b} \frac{(3\lambda^{(i)} + 2G^{(i)})\alpha^{(i)}}{2\lambda^{(i)} + 2G^{(i)}} \frac{\left( \frac{n^2 \pi^2}{b^2} - \frac{m^2 \pi^2}{a^2} \right)}{\beta_{mn}^2}$$

$$SH_{mn}^{(i)}(2, 1) = \frac{2\pi n G^{(i)} e^{\beta_{mn}\bar{z}}}{b} \frac{(3\lambda^{(i)} + 2G^{(i)})\alpha^{(i)}}{2\lambda^{(i)} + 2G^{(i)}} \frac{\left( \frac{n^2 \pi^2}{b^2} - \frac{m^2 \pi^2}{a^2} \right)}{\beta_{mn}^2}$$

$$SH_{mn}^{(i)}(2, 2) = \frac{2\pi n G^{(i)} e^{-\beta_{mn}\bar{z}}}{b} \frac{(3\lambda^{(i)} + 2G^{(i)})\alpha^{(i)}}{2\lambda^{(i)} + 2G^{(i)}} \frac{\left( \frac{n^2 \pi^2}{b^2} - \frac{m^2 \pi^2}{a^2} \right)}{\beta_{mn}^2}$$

$$SH_{mn}^{(i)}(3, 1) = -\frac{2\pi n G^{(i)} e^{\beta_{mn}\bar{z}}}{b} \frac{(3\lambda^{(i)} + 2G^{(i)})\alpha^{(i)}}{2\lambda^{(i)} + 2G^{(i)}}$$

$$SH_{mn}^{(i)}(3, 2) = -\frac{2\pi n G^{(i)} e^{-\beta_{mn} \bar{z}}}{b} \frac{(3\lambda^{(i)} + 2G^{(i)})\alpha^{(i)}}{2\lambda^{(i)} + 2G^{(i)}}$$

$$SH_{mn}^{(i)}(4, 1) = -\frac{mn\pi^2 G^{(i)} e^{\beta_{mn} \bar{z}}}{ab\beta_{mn}} \frac{(3\lambda^{(i)} + 2G^{(i)})\alpha^{(i)}}{\lambda^{(i)} + G^{(i)}}$$

$$SH_{mn}^{(i)}(4, 2) = \frac{mn\pi^2 G^{(i)} e^{-\beta_{mn} \bar{z}}}{ab\beta_{mn}} \frac{(3\lambda^{(i)} + 2G^{(i)})\alpha^{(i)}}{\lambda^{(i)} + G^{(i)}}$$

$$SH_{mn}^{(i)}(5, 1) = -\frac{n^2 \pi^2 G^{(i)} e^{\beta_{mn} \bar{z}}}{b^2 \beta_{mn}} \frac{(3\lambda^{(i)} + 2G^{(i)})\alpha^{(i)}}{\lambda^{(i)} + G^{(i)}}$$

$$SH_{mn}^{(i)}(5, 2) = \frac{n^2 \pi^2 G^{(i)} e^{-\beta_{mn} \bar{z}}}{b^2 \beta_{mn}} \frac{(3\lambda^{(i)} + 2G^{(i)})\alpha^{(i)}}{\lambda^{(i)} + G^{(i)}}$$

$$SH_{mn}^{(i)}(6, 1) = -\frac{2mn^2 \pi^3 G^{(i)} e^{\beta_{mn} \bar{z}}}{ab^2 \beta_{mn}^2} \frac{(3\lambda^{(i)} + 2G^{(i)})\alpha^{(i)}}{\lambda^{(i)} + G^{(i)}}$$

$$SH_{mn}^{(i)}(6, 2) = -\frac{2mn^2 \pi^3 G^{(i)} e^{-\beta_{mn} \bar{z}}}{ab^2 \beta_{mn}^2} \frac{(3\lambda^{(i)} + 2G^{(i)})\alpha^{(i)}}{\lambda^{(i)} + G^{(i)}}$$

## References

- Abdelaziz, H.H., Atmane, H.A., Mechab, I., et al., 2011. Static analysis of functionally graded sandwich plates using an efficient and simple refined theory. *Chin. J. Aeronaut.* 24, 434–448.
- Ahn, C., Liang, X.D., Cai, S.Q., 2019. Bioinspired design of light-powered crawling, squeezing, and jumping untethered soft robot. *Adv. Mater. Technol.* 4 (7), 1900185.
- Ayata, T., Cavusoglu, A., Arcaklioglu, E., 2006. Predictions of temperature distributions on layered metal plates using artificial neural networks. *Energy Convers. Manag.* 47, 2361–2370.
- Baliyan, A., Gaurav, K., Mishra, S.K., 2015. A review of short term load forecasting using artificial neural network models. *Procedia Comput. Sci.* 48, 121–125.
- Bellifa, H., Benrahou, K.H., et al., 2016. Bending and free vibration analysis of functionally graded plates using a simple shear deformation theory and the concept the neutral surface position. *J. Braz. Soc. Mech. Sci. Eng.* 38, 265–275.
- Carrera, E., Brischetto, S., Cinefra, M., Soave, M., 2011. Effects of thickness stretching in functionally graded plates and shells. *Compos. B Eng.* 42, 123–133.
- Choi, S.W., Song, E.J., Hahn, H.T., 2003. Prediction of fatigue damage growth in notched composite laminates using an artificial neural network. *Compos. Sci. Technol.* 63, 661–675.
- Esfe, M.H., Saedodin, S., Sina, N., Afrand, M., 2015. Designing an artificial neural network to predict thermal conductivity and dynamic viscosity of ferromagnetic nanofluid. *Int. Commun. Heat Mass Tran.* 68, 50–57.
- Eslami, M.R., Hetnarski, R.B., Ignaczak, J., Noda, N., 2013. *Theory of Elasticity and Thermal Stresses-Explanations, Problems and Solutions*. Springer Publishing Company, Incorporated, p. 197.
- Ferreira, A., Roque, C., Martins, P., 2003. Analysis of composite plates using higher-order shear deformation theory and a finite point formulation based on the multiquadric radial basis function method. *Compos. B Eng.* 34, 627–636.
- Jia, S., Kari, L., Arteaga, I.L., 2013. A dynamic rotating blade model at an arbitrary stagger angle based on classical plate theory and the Hamilton's principle. *J. Sound Vib.* 332, 1355–1371.
- Jonnalagadda, K.D., Blandford, G.E., Tauchert, T.R., 1994. Piezothermoelastic composite plate analysis using first-order shear deformation theory. *Comput. Struct.* 51, 79–89.
- Keles, D., Scelle, J., Paraschiv, F., Fichtner, W., 2016. Extended forecast methods for day-ahead electricity spot prices applying artificial neural networks. *Appl. Energy* 162, 218–230.
- Koruche, U.S., Patil, S.F., 2015. Application of classical lamination theory and analytical modeling of laminates. *Int. J. Eng. Technol.* 2, 958–965.
- Kumar, J.S., Raju, T.D., Reddy, K., 2011. Bending analysis of composite laminated plates using higher-order shear deformation theory with zig-zag function. *India J. Sci. Technol.* 2, 106–110.
- Liu, H.R., Tian, H.M., Shao, J.Y., Wang, Z.J., Li, X.M., Wang, C.H., Chen, X.L., 2020. An electrically actuated soft artificial muscle based on a high-performance flexible electrothermal film and liquid-crystal elastomer. *ACS Appl. Mater. Interfaces* 12 (50), 56338–56349.
- Lu, H.F., Wang, M., Chen, X.M., Lin, B.P., Yang, H., 2019. Interpenetrating liquid crystal polyurethane/polyacrylate elastomer with ultrastrong mechanical property. *J. Am. Chem. Soc.* 141, 14364–14369.
- Mindlin, R.D., 1951. Influence of rotary inertia and shear on flexural motions of isotropic elastic plates. *J. Appl. Mech.* 18, 31–38.
- Nali, P., Carrera, E., Calvi, A., 2011. Advanced fully coupled thermo-mechanical plate elements for multilayered structures subjected to mechanical and thermal loading. *Int. J. Numer. Methods Eng.* 85, 896–919.
- Nguyen, H.N., Hong, T.T., Vinh, P.V., Quang, N.D., Thom, D.V., 2019. A refined simple first-order shear deformation theory for static bending and free vibration analysis of advanced composite plates. *Materials* 12, 2385.
- Qian, H., Zhou, D., Liu, W.Q., Fang, H., 2014. 3-D elasticity solutions of simply supported laminated rectangular plates in uniform temperature field. *J. Therm. Stresses* 37, 661–677.
- Ramos, I.A., Mantari, J.L., Zenkour, A.M., 2016. Laminated composite plates subject to thermal load using trigonometrical theory based on Carrera Unified Formulation. *Compos. Struct.* 143, 324–335.
- Reddy, B.S., Kumar, J.S., Reddy, K.V.K., 2013. Prediction of deflection and stresses of laminated composite plate with an artificial neural network aid. *Int. J. Appl. Sci. Eng.* 11, 393–413.
- Reddy, B.S., Kumar, J.S., Reddy, C., Reddy, K., 2014. Static analysis of functionally graded plates using higher-order shear deformation theory. *Int. J. Appl. Sci. Eng.* 12, 23–41.
- Sadrnejad, 2009. Vibration equations of thick rectangular plates using mindlin plate theory. *J. Comput. Sci.* 5, 838–842.
- Shimpi, R.P., Guruprasad, P.J., Pakhare, K.S., 2018. Single variable new first-order shear deformation theory for isotropic plates. *Lat. Am. J. Solid. Struct.* 15, e124.
- Vel, S.S., Batra, R.C., 2002. Exact solution for thermoelastic deformations of functionally graded thick rectangular plates. *AIAA J.* 40, 1421–1433.
- Wang, J., Yuan, W.Y., Li, Z.C., Zhu, Y.C., Santos, T., Fan, J.J., 2022. Prediction of mechanical solutions for a laminated LCEs system fusing an analytical model and neural networks. *J. Mech. Behav. Biomed. Mater.* 125, 104918.
- Wu, Kuang-Chong, 2016. Stress intensity factors and energy release rate for anisotropic plates based on the classical plate theory. *Compos. B Eng.* 97, 300–308.
- Xu, Y.P., Zhou, D., Liu, K.F., 2010. Three-dimensional thermoelastic analysis of rectangular plates with variable thickness subjected to thermomechanical loads. *J. Therm. Stresses* 33, 1136–1155.
- Yun, C., Wang, C.J., Sim, K., Chen, J., Li, Y.H., Xing, Y.F., Yu, C.J., Song, J.Z., 2018. A simple analytical thermo-mechanical model for liquid crystal elastomer bilayer structures. *AIP Adv.* 8 (2), 025215.
- Zenkour, M. Ashraf, 2015. Three-dimensional thermal shock plate problem within the framework of different thermoelasticity theories. *Compos. Struct.* 132, 1029–1042.
- Zhang, L.W., Selim, B.A., 2017. Vibration analysis of CNT-reinforced thick laminated composite plates based on Reddy's higher-order shear deformation theory. *Compos. Struct.* 160, 689–705.
- Zhang, L.W., Liew, K.M., Reddy, J.N., 2016. Postbuckling analysis of bi-axially compressed laminated nanocomposite plates using the first-order shear deformation theory. *Compos. Struct.* 152, 418–431.
- Zhang, Z., Zhou, D., Fang, H., Zhang, J.D., Li, X.H., 2021. Analysis of layered rectangular plates under thermo-mechanical loads considering temperature-dependent material properties. *Appl. Math. Model.* 92, 244–260.